Unified formulation of geometrically nonlinear refined beam theories

Unified formulation of geometrically nonlinear refined beam theories

A. Pagani*, E. Carrera†

Mul^2 Team
Department of Mechanical and Aerospace Engineering, Politecnico di Torino
Corso Duca degli Abruzzi 24, 10129 Torino, Italy.

Abstract: *By using the Carrera Unified Formulation (CUF) and a total Lagrangian approach, the unified theory of beams including geometrical nonlinearities is introduced in this paper. According to CUF, kinematics of one-dimensional structures are formulated by employing an index notation and a generalized expansion of the primary variables by arbitrary cross-section functions. Namely, in this work, low- to higher-order beam models with only pure displacement variables are implemented by utilizing Lagrange polynomials expansions of the unknowns on the cross-section. The principle of virtual work and a finite element approximation are used to formulate the governing equations, whereas a Newton-Raphson linearization scheme along with a path-following method based on the arc-length constraint is employed to solve the geometrically nonlinear problem. By using CUF and three-dimensional Green-Lagrange strain components, the explicit forms of the secant and tangent stiffness matrices of the unified beam element are provided in terms of fundamental nuclei, which are invariants of the theory approximation order. A symmetric form of the secant matrix is provided as well by exploiting the linearization of the geometric stiffness terms. Various numerical assessments are proposed, including large deflection analysis, buckling and post-buckling of slender solid cross-section beams. Thin-walled structures are also analysed in order to show the enhanced capabilities of the present formulation. Whenever possible, the results are compared to those from the literature and finite element commercial software tools.*

Keywords: Carrera unified formulation, Higher-order beam theories; Geometrical nonlinearities; Buckling; Post-buckling; Path-following methods.

---

1 Introduction

The elastic, geometrical nonlinear analysis of beam structures has always been a fundamental topic in structural mechanics. Even today, when flexible beams continue to be used for wing structures, space antennas, robotic arms as well as turbine blades among others, the availability of accurate models able to deal with post-buckling and large displacement analysis is of crucial relevance.

*Assistant Professor. Corresponding author. E-mail: alfonso.pagani@polito.it
†Professor of Aerospace Structures and Aeroelasticity

It is well known that for thin and solid cross-section beam structures, an excellent model for geometrically nonlinear analysis is represented by the so-called *elastica* [1, 2, 3] The elastica beam addresses flexural problems by assuming the local curvature as proportional to the bending moment, according to the classical Euler-Bernoulli beam theory [4]. Geometrical nonlinearity is considered and analytical solutions that make use of elliptic integrals are available for clamped-free, clamped-clamped, and simply-supported beams, see [3, 5]. Different boundary conditions, such as clamped-simply supported beams can be addressed for example by perturbation method [6]. Nevertheless, many other numerical approximation procedures have been used in the past and recent years for the resolution of the elastica, see for example the Chebyshev approximation method [7] or the finite difference method [8].

In the presence of torque or spatial frame structures, the analysis has to be generalized to three dimensions [9]. The large deflection analysis of spatial beams is complicated because the successive finite rotations about fixed axes are non-commutative. To circumvent this problem, Argyris *et. al.* [10, 11] introduced the so-called semi-tangential rotations and derived the geometric stiffness matrix of a space beam element using a technique based on natural modes. An updated Lagrangian and a total Lagrangian formulation of a three-dimensional beam element were presented for large displacement and large rotation analysis by Bathe and Bolourchi [12], who pointed out that the updated formulation is computationally more efficient. Although restricted to small strain analysis, several co-rotational formulations were also proposed over the years for the analysis of flexible spatial rods, see for example the work by Crisfield [13]. Based on strain-measures derived from the principle of virtual work as in the pioneering work of Reissner [14], many spatial beam finite elements were formulated, such as in the famous papers of Simo and Vu-Quoc [15, 16], Cardona and Géradin [17] and Ibrahimbegović *et al.* [18]. Interested readers may find helpful the works by Yang *et al.* [19] or Gu and Chan [20], where a more comprehensive review about the state-of-the-art of nonlinear formulations of spatial three-dimensional beam theories can be found.

Many works in the literature are based on the Timoshenko beam theory [21], which assumes a uniform shear distribution along the cross-section of the beam together with the effects of rotatory inertia. Reissner [22], for example, considered the effect of transverse force strains along with the principle of virtual work for the analysis of thin curved beams. The same author discussed the problem of coupled bending torsion deformation of beams in [23, 24]. Pai and Palazzotto [25] used the multiple shooting method for the numerical analysis of various nonlinear elastic cantilever beams including torsional warping effects. Mohyeddin and Fereidoon [26] considered the large displacements of prismatic shear-deformable beams subjected to three-point bending. Gruttmann *et al.* [27] formulated eccentric space curved beams with arbitrary cross-sections based on the Timoshenko beam kinematics and the Green-Lagrange strain measures. In the domain of the variational asymptotic method, the general three-dimensional nonlinear elasticity problem was systematically split into a two-dimensional linear cross-sectional analysis and a one-dimensional nonlinear beam analysis (including, eventually, transverse shear and Vlasov refinements) in several works, see for example Yu *et al.* [28, 29].

The analysis of more complicated problems, such as thin-walled beams subjected to coupling, local effects and other higher-order phenomena, may require the use of evolute and refined beam theories. A comprehensive discussion about higher-order beam models for the linear analysis of metallic structures can be found in the review paper by Carrera *et al.* [30]. Moreover, some detailed expositions of the theories of thin-walled beams before the 1980s can be consulted in the reference texts from Vlasov [31], Bleich [32], Timoshenko and Gere [3] and Murray [33]. The modern literature on the subject is vast and only selected, and

very recent contributions to nonlinear analysis of thin-walled beams are reviewed hereafter, and they are limited to elastic metallic materials and static analysis. For example, by employing a three-dimensional linear elastic model which extends the Saint-Venant solution to non-uniform warping cases, a geometrically nonlinear model for homogeneous and isotropic beams with generic cross-section was implemented by Genoese *et al.* [34] in a co-rotational framework. The Generalized Beam Theory (GBT) was extended to the post-buckling analysis of thin-walled steel frames by Basaglia *et al.* [35] by using the finite element method and incorporating the influence of frame joints. Machado [36] utilized the Ritz method along with the Newton-Raphson linearization scheme to investigate the buckling and post-buckling of thin-walled beams with the aid of a theory which includes bending and warping shear deformability. Mohri et al. [37, 38] developed a seven-degrees-of-freedom beam model able to deal with large torsion, warping, shortening effects as well as flexural-torsional coupling of prismatic and tapered beams with thin-walled members. Based on the boundary element method, Sapountzakis and Tsipiras [39] and Sapountzakis and Dourakopoulos [40] introduced a beam model for torsion and compression analysis of beams with arbitrary cross-section and encompassing various higher-order effects. Vieira *et al.* [41] discussed the geometrically nonlinear analysis of thin-walled structures be employing an higher-order beam model which utilizes the integration over the cross-section of the elasticity equations, appropriately weighted by in-plane approximation functions. Recently, Garcea *et al.* [42] addressed the geometrically nonlinear analysis of beams and shells using solid finite elements and highlighted the advantages of mixed stress/displacement formulations when applied to the path-following analysis and Koiter asymptotic method.

This introductory, short and not comprehensive review reveals a keen interest in the subject and, also, the necessity to bring order in the theories of one-dimensional elastic structures including geometrical nonlinearities. The present research, in fact, aims at introducing an unified beam formulation able to deal with large displacement/rotation analysis of classical as well as complicated and higher-order problems, which include (but are not limited to) in-plane deformations, constrained cross-sectional warping, bending-torsion coupling, localized buckling and nonlinear three-dimensional stress/strain state analysis. Based on the Carrera Unified Formulation (CUF) [43, 44], according to which any theory of structures can degenerate into a generalized kinematics that makes use of an arbitrary expansion of the generalized variables, the nonlinear governing equations and the related finite element arrays of the generic, and eventually hierarchical, geometrically-exact beam theory are written in terms of *fundamental nuclei*. These fundamental nuclei represent the basic building blocks that, when opportunely expanded, allow for the straightforward generation of low- and high-order finite beam elements.

This paper is organized as follows: (i) First, some preliminary and introductory information are given in Section 2, including the constitutive expressions for elastic metallic materials and the Green-Lagrange nonlinear geometrical relations; (ii) Next, CUF and related finite element approximation are briefly introduced in Section 3; (iii) Subsequently, the governing equations are obtained via the principle of virtual work and the linearized, incremental resolution technique with path-following constraint is discussed; (iv) Section 5 provides the explicit forms of the secant and tangent stiffness matrices of the present unified beam element in terms of fundamental nuclei; (v) Then, numerical results, including elastica-like problems as well as thin-walled beams, are discussed to prove the efficacy of the present method; (vi) Finally, the main conclusions are drawn. Also, appendix sections are provided, and they give the components of the stiffness matrices as well as a discussion about the non-symmetry of the secant stiffness matrix.

2 Preliminaries

Consider a beam structure whose cross-section Ω lays on the xz-plane of a Cartesian reference system. As a consequence, the beam axis is placed along y and measures L. The transposed displacement vector is introduced in the following:

$$\mathbf{u}(x,y,z) = \left\{ \begin{array}{ccc} u_x & u_y & u_z \end{array} \right\}^T \tag{1}$$

The stress, $\boldsymbol{\sigma}$, and strain, $\boldsymbol{\epsilon}$, components are expressed in vectorial form with no loss of generality,

$$\boldsymbol{\sigma} = \left\{ \begin{array}{cccccc} \sigma_{xx} & \sigma_{yy} & \sigma_{zz} & \sigma_{xz} & \sigma_{yz} & \sigma_{xy} \end{array} \right\}^T, \quad \boldsymbol{\epsilon} = \left\{ \begin{array}{cccccc} \epsilon_{xx} & \epsilon_{yy} & \epsilon_{zz} & \epsilon_{xz} & \epsilon_{yz} & \epsilon_{xy} \end{array} \right\}^T \tag{2}$$

In this work, linear elastic metallic beam structures are considered. Hence, the Hooke's law providing the constitutive relation holds as follows:

$$\boldsymbol{\sigma} = \mathbf{C}\boldsymbol{\epsilon} \tag{3}$$

where the material matrix $\mathbf{C}$ is

$$\mathbf{C} = \begin{bmatrix} C_{11} & C_{12} & C_{13} & 0 & 0 & 0 \\ C_{12} & C_{22} & C_{23} & 0 & 0 & 0 \\ C_{13} & C_{23} & C_{33} & 0 & 0 & 0 \\ 0 & 0 & 0 & C_{44} & 0 & 0 \\ 0 & 0 & 0 & 0 & C_{55} & 0 \\ 0 & 0 & 0 & 0 & 0 & C_{66} \end{bmatrix} \tag{4}$$

The coefficients of the stiffness matrix depend only on the Young modulus E and the Poisson ratio ν; i.e.

$$\begin{aligned} C_{11} = C_{22} = C_{33} &= \frac{(1-\nu)E}{(1+\nu)(1-\nu)} \\ C_{12} = C_{13} = C_{23} &= \frac{\nu\, E}{(1+\nu)(1-\nu)} \\ C_{44} = C_{55} = C_{66} &= \frac{E}{2(1+\nu)} \end{aligned} \tag{5}$$

As far as the geometrical relations are concerned, the Green-Lagrange nonlinear strain components are considered. Therefore, the displacement-strain relations are expressed as

$$\boldsymbol{\epsilon} = \boldsymbol{\epsilon}_l + \boldsymbol{\epsilon}_{nl} = (\mathbf{b}_l + \mathbf{b}_{nl})\mathbf{u} \tag{6}$$

where $\mathbf{b}_l$ and $\mathbf{b}_{nl}$ are the linear and nonlinear differential operators, respectively. For the sake

of completeness, these operators are given below.

$$\mathbf{b}_l = \begin{bmatrix} \partial_x & 0 & 0 \\ 0 & \partial_y & 0 \\ 0 & 0 & \partial_z \\ \partial_z & 0 & \partial_x \\ 0 & \partial_z & \partial_y \\ \partial_y & \partial_x & 0 \end{bmatrix}, \qquad \mathbf{b}_{nl} = \begin{bmatrix} \frac{1}{2}(\partial_x)^2 & \frac{1}{2}(\partial_x)^2 & \frac{1}{2}(\partial_x)^2 \\ \frac{1}{2}(\partial_y)^2 & \frac{1}{2}(\partial_y)^2 & \frac{1}{2}(\partial_y)^2 \\ \frac{1}{2}(\partial_z)^2 & \frac{1}{2}(\partial_z)^2 & \frac{1}{2}(\partial_z)^2 \\ \partial_x\,\partial_z & \partial_x\,\partial_z & \partial_x\,\partial_z \\ \partial_y\,\partial_z & \partial_y\,\partial_z & \partial_y\,\partial_z \\ \partial_x\,\partial_y & \partial_x\,\partial_y & \partial_x\,\partial_y \end{bmatrix} \tag{7}$$

where $\partial_x = \dfrac{\partial(\cdot)}{\partial x}$, $\partial_y = \dfrac{\partial(\cdot)}{\partial y}$, and $\partial_z = \dfrac{\partial(\cdot)}{\partial z}$.

3 Unified finite beam element

3.1 Carrera Unified Formulation

Within the framework of the Carrera Unified Formulation (CUF), the three-dimensional displacement field $\mathbf{u}(x, y, z)$ can be expressed as a general expansion of the primary unknowns. In the case of one-dimensional theories, one has:

$$\mathbf{u}(x, y, z) = F_s(x, z)\mathbf{u}_s(y), \qquad s = 1, 2, ..., M \tag{8}$$

where F_s are the functions of the coordinates x and z on the cross-section, $\mathbf{u}_s$ is the vector of the *generalized* displacements which lay along the beam axis, M stands for the number of the terms used in the expansion, and the repeated subscript s indicates summation. The choice of F_s determines the class of the 1D CUF model that is required and subsequently to be adopted.

In this paper, Lagrange polynomials are used as F_s cross-sectional functions. The resulting beam theories are known to as LE (Lagrange Expansion) CUF models in the literature [44]. LE models utilize only pure displacements as primary unknowns and they have been recently used for the component-wise analysis of aerospace and civil engineering constructions as well as for composite laminates and box structures, see [45, 46, 47, 48, 49, 50]. Lagrange polynomials as used in this paper can be found in [51]. In the framework of CUF, linear three- (L3) and four-point (L4), quadratic six- (L6) and nine-point (L9), as well as cubic 16-point (L16) Lagrange polynomials have been used to formulate linear to higher-order kinematics beam models. For a further improvement of the beam kinematics and a geometrically correct (isoparametric) description of complex cross-section beams, a combination of Lagrange polynomials can be used in a straightforward manner by employing CUF. For more details about LE beam theories, the readers are referred to the original paper by Carrera and Petrolo [52].

3.2 Finite element formulation

The Finite Element Method (FEM) is adopted to discretize the structure along the y-axis. Thus, the generalized displacement vector $\mathbf{u}_s(y)$ is approximated as follows:

$$\mathbf{u}_s(y) = N_j(y)\mathbf{q}_{sj} \qquad j = 1, 2, \ldots, p+1 \tag{9}$$

where N_j stands for the j-th shape function, p is the order of the shape functions and j indicates summation. $\mathbf{q}_{sj}$ is the following vector of the FE nodal parameters:

$$\mathbf{q}_{sj} = \left\{ \begin{array}{ccc} q_{x_{sj}} & q_{y_{sj}} & q_{z_{sj}} \end{array} \right\}^T \tag{10}$$

For the sake of brevity, the shape functions N_j are not reported here. They can be found in many reference texts, for instance in Bathe [51]. However, it should be underlined that the choice of the cross-section polynomials sets for the LE kinematics (i.e. the selection of the type, the number and the distribution of cross-sectional polynomials) is completely independent of the choice of the beam finite element to be used along the beam axis. In this work, classical one-dimensional finite elements with four nodes (B4) are adopted, i.e. a cubic approximation along the y-axis is assumed.

4 Nonlinear governing equations

4.1 Equilibrium

Consider an elastic system in equilibrium under applied forces and some prescribed geometrical constraints. The principle of virtual work states that *the sum of all the virtual work done by the internal and external forces existing in the system in any arbitrary infinitesimal virtual displacements satisfying the prescribed geometrical constraints is zero* [53]. Namely,

$$\delta L_{\text{int}} - \delta L_{\text{ext}} = 0 \tag{11}$$

where L_{int} is the strain energy, L_{ext} is the work of the external loadings, and δ denotes the variation.

Large deflection analysis of elastic systems results in complex nonlinear differential problems, whose analytical solution is available rarely and limited to a narrow range of applications. The resolution of the geometrically nonlinear elasticity and related theories of structures can be extended to a much wider class of problems if FEM is employed. In this case, in fact, the equilibrium condition of the structure can be expressed as a system of nonlinear algebraic equations. Moreover, if CUF (Eq. (8)) is utilized along with Eqs. (9) and (11), the equilibrium conditions and the related finite element arrays of the generic structural theory can be written in a simple and unified manner as follows:

$$\mathbf{K}_S^{ij\tau s}\,\mathbf{q}_{sj} - \mathbf{p}_{sj} = 0 \tag{12}$$

Equation (12) represents a set of three algebraic equations, where $\mathbf{p}_{sj}$ and $\mathbf{K}_S^{ij\tau s}$ are the *Fundamental Nuclei* (FNs) of the vector of the nodal loadings and the *secant* stiffness matrix, respectively. The derivation of the FN of the loading vector is not reported in this paper, but it can be found in [43]. On the other hand, the detailed formulation of the FN of the nonlinear secant stiffness matrix is discussed in Section 5.1.

Although the content of this section can be easily generalized to two-dimensional structural models (i.e., plates and shells) as well as three-dimensional elasticity, this paper primarily

addresses beam theories based on CUF, according to which the finite element governing equations of the generic, arbitrary higher-order model can be automatically obtained by expanding Eq. (12) and the related FNs versus the indexes $\tau, s = 1, ..., M$ and $i, j = 1, ..., p+1$ to give

$$\mathbf{K}_S\,\mathbf{q} - \mathbf{p} = 0 \tag{13}$$

where $\mathbf{K}_S$, $\mathbf{q}$, and $\mathbf{p}$ are global, assembled finite element arrays of the final structure. For more details about the expansion of the FNs and the finite element assembly procedure in the framework of CUF, the readers are referred to Carrera *et al.* [44].

4.2 Newton-Raphson linearization with path-following constraint

Equation (13) constitutes the starting point for finite element calculation of geometrically nonlinear systems, and it is usually solved through an incremental linearized scheme, typically the Newton-Raphson method (or *tangent method*). According to the Newton-Raphson method, Eq. (13) is written as [54]:

$$\boldsymbol{\varphi}_{res} \equiv \mathbf{K}_S\,\mathbf{q} - \mathbf{p} = 0 \tag{14}$$

where $\boldsymbol{\varphi}_{res}$ is the vector of the *residual nodal forces* (unbalanced nodal force vector). Equation (14) can now be linearized by expanding $\boldsymbol{\varphi}_{res}$ in Taylor's series about a known solution $(\mathbf{q}, \mathbf{p})$. Omitting the second-order terms, one has

$$\boldsymbol{\varphi}_{res}(\mathbf{q} + \delta\mathbf{q}, \mathbf{p} + \delta\mathbf{p}) = \boldsymbol{\varphi}_{res}(\mathbf{q}, \mathbf{p}) + \frac{\partial \boldsymbol{\varphi}_{res}}{\partial \mathbf{q}}\,\delta\mathbf{q} + \frac{\partial \boldsymbol{\varphi}_{res}}{\partial \mathbf{p}}\,\delta\lambda\,\mathbf{p}_{ref} = 0 \tag{15}$$

where $\dfrac{\partial \boldsymbol{\varphi}_{res}}{\partial \mathbf{q}} = \mathbf{K}_T$ is the *tangent* stiffness matrix, and $-\dfrac{\partial \boldsymbol{\varphi}_{res}}{\partial \mathbf{p}}$ is equal to the unit matrix $\mathbf{I}$. In Eq. (15) it has been assumed that the load varies directly with the vector of the reference loadings $\mathbf{p}_{ref}$ and has a rate of change equal to the load parameter λ, i.e. $\mathbf{p} = \lambda\,\mathbf{p}_{ref}$. Equation (15) is written in a more compact form as follows:

$$\mathbf{K}_T\,\delta\mathbf{q} = \delta\lambda\,\mathbf{p}_{ref} - \boldsymbol{\varphi}_{res} \tag{16}$$

Since the load-scaling parameter λ is taken as a variable, an additional governing equation is required and this is given by a constraint relationship $c(\delta\mathbf{q}, \delta\lambda)$ to finally give

$$\begin{cases} \mathbf{K}_T\,\delta\mathbf{q} = \delta\lambda\,\mathbf{p}_{ref} - \boldsymbol{\varphi}_{res} \\ \\ c(\delta\mathbf{q}, \delta\lambda) = 0 \end{cases} \tag{17}$$

Depending on the constraint equation, different incremental schemes can be implemented. For example, if the constraint equation is $\delta\lambda = 0$, Eq. (17) corresponds to a load-control method. On the other hand, the condition $c(\delta\mathbf{q}, \delta\lambda) = \delta\mathbf{q} = 0$ represents a displacement-control method. In this paper, a path-following method is employed in which the constraint equation is a function of both displacement and load parameter variations. Differences between load- and displacement-control methods as well as path-following methods are briefly depicted in Fig. 1 and more details can be found in [54, 55, 56].

Geometry and notations of the incremental scheme as employed in this work is introduced in detail in Fig. 2. In this figure, finite variations are referred to as $\delta^n_m(\cdot)$, where $m = 1, 2, ...$

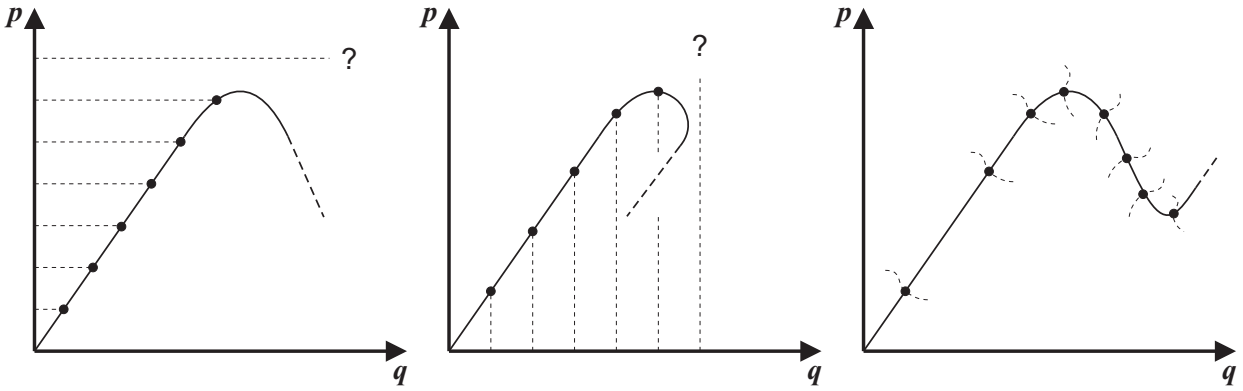

(a) Load-control method (b) Displacement-control method (c) Path-following method

Figure 1: Representation and meaning of the constraint governing equation, $c(\delta\mathbf{q}, \delta\lambda)$, see [55].

denotes the global variations of the load-step[1] and $n = 0, 1, 2, ...$ denotes the local iteration within the load-step m, such that $\delta^n_m(\cdot) = (\cdot)^n_m - (\cdot)^{n-1}_m$ and $(\cdot)_m = (\cdot)_{m-1} + \sum_n \delta^n_m(\cdot)$. $n = 0$ and consequently $\delta^0_m\mathbf{q}$ correspond to the initial solution (the linear solution in the case $m = 1$); $\delta^0_m\lambda$ is the initial increment of the load parameter; $\mathbf{q}_{m-1}$ and $\lambda_{m-1}\,\mathbf{p}_{ref}$ are, respectively, the displacement and load vectors at the previous load-step; and $\boldsymbol{\varphi}^n_{m_{res}}$ is the residual force vector at the current iteration. In Fig. 2 and according to Eq. (17), the equilibrium iterates (solid dots) are given by the intersection of the linearized governing equations and the constraint equation $c(\delta\mathbf{q}, \delta\lambda) = 0$, which is depicted as a series of arcs. At each iteration, $\mathbf{t}^n_m = \mathbf{t}^{n-1}_m + \delta^n_m\mathbf{t} = \mathbf{t}^{n-1}_m + (\delta^n_m\mathbf{q} + \delta^n_m\lambda\,\mathbf{p}_{ref})$ is the vector connecting the current equilibrium iterates with the solution at the previous load-step.

Because the arc-length method as proposed by Criefield [57, 58] is utilized, the constraint relationship corresponds to a multi-dimensional sphere with radius equal to the given initial arch-length value Δl^0_m. As a consequence, this means that the modulus of vector $\mathbf{t}$ at the generic iteration, i.e. $|\mathbf{t}^n_m|$, must be equal to the square of the arc-length. Formally, Eq. (17) becomes

$$\begin{cases} \mathbf{K}_T\,\delta^n_m\mathbf{q} = \delta^n_m\lambda\,\mathbf{p}_{ref} - \boldsymbol{\varphi}^n_{m_{res}} \\ \\ {\mathbf{t}^n_m}^T\mathbf{t}^n_m = (\Delta l^0_m)^2 \end{cases} \tag{18}$$

In order to preserve symmetric solvers proper of finite element codes and to avoid the computation of the inverse of the tangent matrix, the Batoz and Dhatt [59] strategy is adopted and the incremental displacement vector at the current iteration is expressed as follows:

$$\delta^n_m\mathbf{q} = \delta^n_m\lambda\,\bar{\mathbf{q}}^n_m + \delta^n_m\hat{\mathbf{q}} \tag{19}$$

where $\bar{\mathbf{q}}^n_m$ and $\delta^n_m\hat{\mathbf{q}}$ are the solutions of the following linear systems:

$$\begin{cases} \mathbf{K}_T\,\bar{\mathbf{q}}^n_m = \mathbf{p}_{ref} \\ \\ \mathbf{K}_T\,\delta^n_m\hat{\mathbf{q}} = -\boldsymbol{\varphi}^n_{m_{res}} \end{cases} \tag{20}$$

Thus, according to Crisfield [57] and by substituting Eq. (19) into the second of Eq. (18), the

[1]The term *load-step* is extensively adopted even if a mixed load-displacement constraint equation will be utilized.

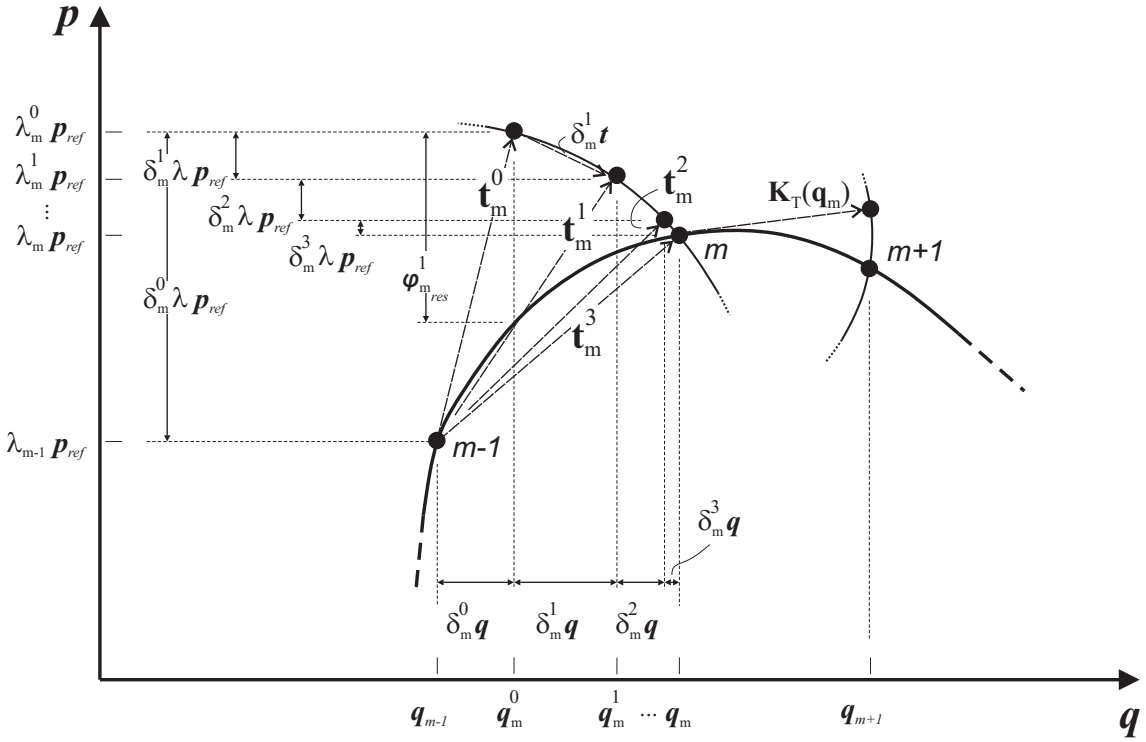

Figure 2: Geometry and notation in the incremental scheme.

following quadratic constraint equation arises:

$$a\,(\delta_m^n\lambda)^2 + 2\,b\,\delta_m^n\lambda + c = 0 \tag{21}$$

where

$$\begin{aligned} a &= \bar{\mathbf{q}}_m^{n^T}\,\bar{\mathbf{q}}_m^n + \mathbf{p}_{ref}^T\,\mathbf{p}_{ref} \\ b &= (\mathbf{q}_m^{n-1} - \mathbf{q}_{m-1})^T\,\bar{\mathbf{q}}_m^n + \bar{\mathbf{q}}_m^{n^T}\,\delta_m^n\hat{\mathbf{q}} + (\lambda_m^{n-1} - \lambda_{m-1})\,\mathbf{p}_{ref}^T\mathbf{p}_{ref} \\ c &= \left((\mathbf{q}_m^{n-1} - \mathbf{q}_{m-1}) + \delta_m^n\hat{\mathbf{q}}\right)^T\left((\mathbf{q}_m^{n-1} - \mathbf{q}_{m-1}) + \delta_m^n\hat{\mathbf{q}}\right) + \\ &\quad (\lambda_m^{n-1} - \lambda_{m-1})^2\,\mathbf{p}_{ref}^T\mathbf{p}_{ref} - (\Delta l_m^0)^2 \end{aligned} \tag{22}$$

For numerical (and physical) reasons, Crisfield proposed to neglect the terms related to the load term $\mathbf{p}_{ref}$ from Eq. (22).

Equation (21) gives two different solutions for the variation of the load parameter $\delta_m^n\lambda$. To avoid *doubling back* on the original load-deflection path, various authors proposed different shortcomings. For example, Crisfield [57] proposed to choose the appropriate root by evaluating the two angles between the vectors $\mathbf{t}_m^{n-1}$, before the current iteration, and the vector $\mathbf{t}_m^n$, at the current iteration and calculated by using the two different roots of Eq. (21). The appropriate solution is the one that gives a positive angle, unless both angles are positive. In that case, the appropriate root is the one closest to the linear solution of Eq. (21), i.e. $\delta_m^n\lambda = -\dfrac{c}{b}$. In this work and as proposed by Carrera [55], between the two solutions of Eq. (21) we choose the one which is closest to the solution of the *consistent-linearized* constraint equation, $\delta_m^n\lambda_{\rm cl}$. $\delta_m^n\lambda_{\rm cl}$ is calculated by linearizing the constraint relationship $c(\delta\mathbf{q}, \delta\lambda) = 0$ in the same manner of the equilibrium equations (Eqs. (13) to (16)). In this sense the solution is referred to as *consistent*, see Schweizerhof and Wriggers [60]. The consistent linearization of the constraint

equation and the related solution is not reported here for the sake of brevity, but it can be found in [55].

Before discussing the formulation of the nonlinear stiffness matrices of the unified beam element, it is important to underline a couple of aspects. In this research, we employ a *full* Newton-Raphson method that, as opposed to a *modified* scheme, utilizes an updated tangent stiffness matrix at each iteration. As it will be clear later in this paper and unlike $\mathbf{K}_S$, the calculation of the tangent stiffness matrix $\mathbf{K}_T$ is not trivial, and it comes from the linearization of the constitutive equations and the geometrical relations. Moreover, although it is not the case of the problems addressed in this paper, the formulation of $\mathbf{K}_T$ in consistent closed-form is not necessarily available (e.g., in the case of nonelastic problems and fluid-structure interaction), see Wriggers and Simo [61]. On the other hand, it can be observed that alternative "directions" instead of $\mathbf{K}_T$ can be employed for the approximate solution of the linearized system of Eqs. (18) and (20). In the *secant method*, for example, the secant stiffness matrix $\mathbf{K}_S$ is used [62]. The main disadvantages of employing $\mathbf{K}_S$ into Eq. (20) is that the secant stiffness matrix is not uniquely defined, is generally non-symmetric, and results in resolution methods with low orders of convergence (approximately 1.6 against 2 of tangent methods[2]). In this work, if not differently specified, the tangent stiffness matrix is used to formulate the linearized iterative scheme and the secant stiffness matrix is utilized merely for evaluating the equilibrium defect and the residual at each iteration, i.e. $\boldsymbol{\varphi}^n_{m_{res}}$. Therefore, by referring to a *total Lagrangian* formulation, the expressions of both $\mathbf{K}_S$ and $\mathbf{K}_T$ are provided. These matrices are given in terms of FNs which, according to CUF, allow to engender the element matrices of any arbitrary refined and classical beam theories. For the sake of completeness, also a symmetric form of the fundamental nucleus of the secant stiffness matrix is provided in an appendix section.

5 Explicit forms of secant and tangent matrices

5.1 Fundamental nucleus of the secant stiffness matrix

The secant stiffness matrix $\mathbf{K}_S$ can be calculated from the virtual variation of the strain energy δL_{int}, which reads:

$$\delta L_{\text{int}} = < \delta \boldsymbol{\epsilon}^T \boldsymbol{\sigma} > \tag{23}$$

where $< (\cdot) >= \int_V (\cdot)\, dV$. Under the hypothesis of small deformations, $V = \Omega \times L$ is the initial volume of the beam structure.

The strain vector $\boldsymbol{\epsilon}$ in Eq. (6) can be written in terms of the generalized nodal unknowns $\mathbf{q}_{sj}$ by employing Eqs. (8) and (9).

$$\boldsymbol{\epsilon} = (\mathbf{B}^{sj}_l + \mathbf{B}^{sj}_{nl})\mathbf{q}_{sj} \tag{24}$$

[2]This is not true in the case of *modified* Newton-Raphson schemes, where $\mathbf{K}_T$ is updated only at the first iteration of each load step.

where $\mathbf{B}_l^{sj}$ and $\mathbf{B}_{nl}^{sj}$ are the two following matrices:

$$\mathbf{B}_l^{sj} = \mathbf{b}_l(F_s\, N_j) = \begin{bmatrix} F_{s,x}N_j & 0 & 0 \\ 0 & F_s N_{j,y} & 0 \\ 0 & 0 & F_{s,z}N_j \\ F_{s,z}N_j & 0 & F_{s,x}N_j \\ 0 & F_{s,z}N_j & F_s N_{j,y} \\ F_s N_{j,y} & F_{s,x}N_j & 0 \end{bmatrix} \tag{25}$$

and

$$\mathbf{B}_{nl}^{sj} = \frac{1}{2}\begin{bmatrix} u_{x,x}F_{s,x}N_j & u_{y,x}F_{s,x}N_j & u_{z,x}F_{s,x}N_j \\ u_{x,y}F_s N_{j,y} & u_{y,y}F_s N_{j,y} & u_{z,y}F_s N_{j,y} \\ u_{x,z}F_{s,z}N_j & u_{y,z}F_{s,z}N_j & u_{z,z}F_{s,z}N_j \\ u_{x,x}F_{s,z}N_j + u_{x,z}F_{s,x}N_j & u_{y,x}F_{s,z}N_j + u_{y,z}F_{s,x}N_j & u_{z,x}F_{s,z}N_j + u_{z,z}F_{s,x}N_j \\ u_{x,y}F_{s,z}N_j + u_{x,z}F_s N_{j,y} & u_{y,y}F_{s,z}N_j + u_{y,z}F_s N_{j,y} & u_{z,y}F_{s,z}N_j + u_{z,z}F_s N_{j,y} \\ u_{x,x}F_s N_{j,y} + u_{x,y}F_{s,x}N_j & u_{y,x}F_s N_{j,y} + u_{y,y}F_{s,x}N_j & u_{z,x}F_s N_{j,y} + u_{z,y}F_{s,x}N_j \end{bmatrix} \tag{26}$$

In Eqs. (25) and (26), commas denote partial derivatives. It is easy to verify that, analogously to Eq. (24), the virtual variation of the strain vector $\delta\boldsymbol{\epsilon}$ can be written in terms of nodal unknowns as follows:

$$\delta\boldsymbol{\epsilon} = \delta\big((\mathbf{B}_l^{\tau i} + \mathbf{B}_{nl}^{\tau i})\mathbf{q}_{\tau i}\big) = (\mathbf{B}_l^{\tau i} + 2\mathbf{B}_{nl}^{\tau i})\delta\mathbf{q}_{\tau i} \tag{27}$$

Thus,

$$\delta\boldsymbol{\epsilon}^T = \delta\mathbf{q}_{\tau i}^T(\mathbf{B}_l^{\tau i} + 2\,\mathbf{B}_{nl}^{\tau i})^T \tag{28}$$

In writing Eqs. (27) and (28), the indexes τ and i have been respectively used instead of s and j for the sake of convenience.

Now, Eqs. (3), (24) and (28) can be substituted into Eq. (23) to have

$$\begin{aligned} \delta L_{\text{int}} &= \delta\mathbf{q}_{\tau i}^T < \left(\mathbf{B}_l^{\tau i} + 2\,\mathbf{B}_{nl}^{\tau i}\right)^T \mathbf{C}\left(\mathbf{B}_l^{sj} + \mathbf{B}_{nl}^{sj}\right) > \mathbf{q}_{sj} \\ &= \delta\mathbf{q}_{\tau i}^T\,\mathbf{K}_0^{ij\tau s}\,\mathbf{q}_{sj} + \delta\mathbf{q}_{\tau i}^T\,\mathbf{K}_{lnl}^{ij\tau s}\,\mathbf{q}_{sj} + \delta\mathbf{q}_{\tau i}^T\,\mathbf{K}_{nll}^{ij\tau s}\,\mathbf{q}_{sj} + \delta\mathbf{q}_{\tau i}^T\,\mathbf{K}_{nlnl}^{ij\tau s}\,\mathbf{q}_{sj} \\ &= \delta\mathbf{q}_{\tau i}^T\,\mathbf{K}_S^{ij\tau s}\,\mathbf{q}_{sj} \end{aligned} \tag{29}$$

where the secant stiffness matrix is $\mathbf{K}_S^{ij\tau s} = \mathbf{K}_0^{ij\tau s} + \mathbf{K}_{lnl}^{ij\tau s} + \mathbf{K}_{nll}^{ij\tau s} + \mathbf{K}_{nlnl}^{ij\tau s}$. In Eq. (29), $\mathbf{K}_0^{ij\tau s}$ is the linear component of $\mathbf{K}_S$ (i.e., it is the linear stiffness matrix), $\mathbf{K}_{lnl}^{ij\tau s}$ and $\mathbf{K}_{nll}^{ij\tau s}$ represent

the nonlinear contributions of order 1, and $\mathbf{K}_{nlnl}^{ij\tau s}$ contains the nonlinearities of order 2. They are clearly given by:

$$\begin{aligned} \mathbf{K}_{0}^{ij\tau s} &=< (\mathbf{B}_{l}^{\tau i})^{T}\mathbf{C}\,\mathbf{B}_{l}^{sj} > \qquad \mathbf{K}_{lnl}^{ij\tau s} =< (\mathbf{B}_{l}^{\tau i})^{T}\mathbf{C}\,\mathbf{B}_{nl}^{sj} > \\ \mathbf{K}_{nll}^{ij\tau s} &= 2 < (\mathbf{B}_{nl}^{\tau i})^{T}\mathbf{C}\,\mathbf{B}_{l}^{sj} > \quad \mathbf{K}_{nlnl}^{ij\tau s} = 2 < (\mathbf{B}_{nl}^{\tau i})^{T}\mathbf{C}\,\mathbf{B}_{nl}^{sj} > \end{aligned} \tag{30}$$

For the sake of completeness, the expressions of matrices in Eq. (30) are given in Appendix A. Matrices $\mathbf{K}_{0}^{ij\tau s}$, $\mathbf{K}_{lnl}^{ij\tau s}$, $\mathbf{K}_{nll}^{ij\tau s}$, and $\mathbf{K}_{nlnl}^{ij\tau s}$ are given in terms of *fundamental nuclei*. These are 3×3 matrices that, given the cross-sectional functions ($F_\tau = F_s$, for $\tau = s$) and the shape functions ($N_i = N_j$, for $i = j$), can be expanded by using the indexes $\tau, s = 1, ..., M$ and $i, j = 1, ..., p+1$ in order to obtain the elemental secant stiffness matrix of any arbitrarily refined beam model. In other words, by opportunely choosing the beam kinematics (i.e., by choosing F_τ as well as the number of expansion terms M) classical to higher-order beam theories and related secant stiffness arrays can be implemented in an automatic manner by exploiting the index notation of CUF. Once the elemental secant stiffness matrix is obtained, it can be assembled in the classical way of FEM, see [44].

It is of relevant importance to note that $\mathbf{K}_S$ as given in this section is not symmetric. The non-symmetry of the secant stiffness matrix may result in mathematical and practical drawbacks which are discussed in Appendix B. In the same appendix section, a symmetric form of the secant stiffness matrix that makes use of the linearization of the geometric stiffness terms is developed for the sake of completeness.

5.2 Fundamental nucleus of the tangent stiffness matrix

The fundamental nucleus of the tangent stiffness matrix $\mathbf{K}_{T}^{ij\tau s}$ is derived from the linearization of the equilibrium equations [63], see Eq. (15). We assume that the loading is conservative so that the linearization of the virtual variation of the external loads is null, i.e. $\delta(\delta L_{\text{ext}}) = 0$. Thus, the only terms to be linearized are the strain-displacement operators and the stress-strain relations. In fact, the tangent matrix can be formally obtained from linearizing the virtual variation of the strain energy as follows:

$$\begin{aligned} \delta(\delta L_{\text{int}}) &= < \delta(\delta\boldsymbol{\epsilon}^{T}\boldsymbol{\sigma}) > \\ &= < \delta\boldsymbol{\epsilon}^{T}\delta\boldsymbol{\sigma} > + < \delta(\delta\boldsymbol{\epsilon}^{T})\boldsymbol{\sigma} > \\ &= \delta\mathbf{q}_{\tau i}^{T}(\mathbf{K}_{0}^{ij\tau s} + \mathbf{K}_{T_1}^{ij\tau s} + \mathbf{K}_{\sigma}^{ij\tau s})\delta\mathbf{q}_{sj} \\ &= \delta\mathbf{q}_{\tau i}^{T}\mathbf{K}_{T}^{ij\tau s}\delta\mathbf{q}_{sj} \end{aligned} \tag{31}$$

Each nonlinear contribution in the right-hand-side of Eq. (31), i.e. $\mathbf{K}_{T_1}^{ij\tau s}$ and $\mathbf{K}_{\sigma}^{ij\tau s}$, is now considered separately. The first term, $< \delta\boldsymbol{\epsilon}^{T}\delta\boldsymbol{\sigma} >$, demands for the linearization of the constitutive relations (Eq. (3)), which, under the hypothesis of constant material coefficients (i.e., $\delta\mathbf{C} = 0$) and according to Eq. (27), hold

$$\delta\boldsymbol{\sigma} = \delta(\mathbf{C}\boldsymbol{\epsilon}) = \mathbf{C}\delta\boldsymbol{\epsilon} = \mathbf{C}(\mathbf{B}_{l}^{sj} + 2\,\mathbf{B}_{nl}^{sj})\delta\mathbf{q}_{sj} \tag{32}$$

Hence, considering Eqs. (28) and (32), one has:

$$
\begin{aligned}
< \delta\boldsymbol{\epsilon}^T \delta\boldsymbol{\sigma} > &= \delta\mathbf{q}_{\tau i}^T < (\mathbf{B}_l^{\tau i} + 2\,\mathbf{B}_{nl}^{\tau i})^T \mathbf{C}\,(\mathbf{B}_l^{sj} + 2\,\mathbf{B}_{nl}^{sj}) > \delta\mathbf{q}_{sj} \\
&= \delta\mathbf{q}_{\tau i}^T\,\mathbf{K}_0^{ij\tau s}\,\delta\mathbf{q}_{sj} + \delta\mathbf{q}_{\tau i}^T\left(2\,\mathbf{K}_{lnl}^{ij\tau s}\right)\delta\mathbf{q}_{sj} + \delta\mathbf{q}_{\tau i}^T\,\mathbf{K}_{nll}^{ij\tau s}\,\delta\mathbf{q}_{sj} + \delta\mathbf{q}_{\tau i}^T\left(2\,\mathbf{K}_{nlnl}^{ij\tau s}\right)\delta\mathbf{q}_{sj} \\
&= \delta\mathbf{q}_{\tau i}^T\left(\mathbf{K}_0^{ij\tau s} + \mathbf{K}_{T_1}^{ij\tau s}\right)\delta\mathbf{q}_{sj}
\end{aligned}
\tag{33}
$$

where $\mathbf{K}_{T_1}^{ij\tau s} = 2\,\mathbf{K}_{lnl}^{ij\tau s} + \mathbf{K}_{nll}^{ij\tau s} + 2\,\mathbf{K}_{nlnl}^{ij\tau s}$ is the nonlinear contribution of the fundamental nucleus of the tangent stiffness matrix due to the linearization of the Hooke's law. $\mathbf{K}_0^{ij\tau s}$, $\mathbf{K}_{lnl}^{ij\tau s}$, $\mathbf{K}_{nll}^{ij\tau s}$, and $\mathbf{K}_{nlnl}^{ij\tau s}$ are the same 3×3 FNs as given in Eq. (30) and Appendix A. It is interesting to note that, unlike $\mathbf{K}_S$, $\mathbf{K}_0$ and $\mathbf{K}_{T_1}$ coming from the expansion of the relative nuclei are symmetric matrices.

The evaluation of the second contribution in the right-hand-side of Eq. (31), i.e. $< \delta(\delta\boldsymbol{\epsilon}^T)\boldsymbol{\sigma} >$, requires the linearization of the nonlinear geometrical relations. According to Crisfield [56] and from Eqs. (6) and (7),

$$
\delta(\delta\boldsymbol{\epsilon}) = \left\{ \begin{array}{c}
\left(\delta u_{x_{,x}}\right)_{\mathrm{v}} \delta u_{x_{,x}} + \left(\delta u_{y_{,x}}\right)_{\mathrm{v}} \delta u_{y_{,x}} + \left(\delta u_{z_{,x}}\right)_{\mathrm{v}} \delta u_{z_{,x}} \\
\left(\delta u_{x_{,y}}\right)_{\mathrm{v}} \delta u_{x_{,y}} + \left(\delta u_{y_{,y}}\right)_{\mathrm{v}} \delta u_{y_{,y}} + \left(\delta u_{z_{,y}}\right)_{\mathrm{v}} \delta u_{z_{,y}} \\
\left(\delta u_{x_{,z}}\right)_{\mathrm{v}} \delta u_{x_{,z}} + \left(\delta u_{y_{,z}}\right)_{\mathrm{v}} \delta u_{y_{,z}} + \left(\delta u_{z_{,z}}\right)_{\mathrm{v}} \delta u_{z_{,z}} \\
\left[\left(\delta u_{x_{,x}}\right)_{\mathrm{v}} \delta u_{x_{,z}} + \delta u_{x_{,x}} \left(\delta u_{x_{,z}}\right)_{\mathrm{v}}\right] + \left[\left(\delta u_{y_{,x}}\right)_{\mathrm{v}} \delta u_{y_{,z}} + \delta u_{y_{,x}} \left(\delta u_{y_{,z}}\right)_{\mathrm{v}}\right] + \left[\left(\delta u_{z_{,x}}\right)_{\mathrm{v}} \delta u_{z_{,z}} + \delta u_{z_{,x}} \left(\delta u_{z_{,z}}\right)_{\mathrm{v}}\right] \\
\left[\left(\delta u_{x_{,y}}\right)_{\mathrm{v}} \delta u_{x_{,z}} + \delta u_{x_{,y}} \left(\delta u_{x_{,z}}\right)_{\mathrm{v}}\right] + \left[\left(\delta u_{y_{,y}}\right)_{\mathrm{v}} \delta u_{y_{,z}} + \delta u_{y_{,y}} \left(\delta u_{y_{,z}}\right)_{\mathrm{v}}\right] + \left[\left(\delta u_{z_{,y}}\right)_{\mathrm{v}} \delta u_{z_{,z}} + \delta u_{z_{,y}} \left(\delta u_{z_{,z}}\right)_{\mathrm{v}}\right] \\
\left[\left(\delta u_{x_{,x}}\right)_{\mathrm{v}} \delta u_{x_{,y}} + \delta u_{x_{,x}} \left(\delta u_{x_{,y}}\right)_{\mathrm{v}}\right] + \left[\left(\delta u_{y_{,x}}\right)_{\mathrm{v}} \delta u_{y_{,y}} + \delta u_{y_{,x}} \left(\delta u_{y_{,y}}\right)_{\mathrm{v}}\right] + \left[\left(\delta u_{z_{,x}}\right)_{\mathrm{v}} \delta u_{z_{,y}} + \delta u_{z_{,x}} \left(\delta u_{z_{,y}}\right)_{\mathrm{v}}\right]
\end{array} \right\}
\tag{34}
$$

where the subscript "v" denotes the variations. It is easy to verify the following matricial form of Eq. (34) by employing CUF (8) and the finite element approximation (9) for both the linearized variables (i.e., $\delta\mathbf{u} = F_s N_j \delta\mathbf{q}_{sj}$) and the variations (i.e., $(\delta\mathbf{u})_{\mathrm{v}} = F_\tau N_i \delta\mathbf{q}_{\tau i}$):

$$
\delta(\delta\boldsymbol{\epsilon}) = \mathbf{B}_{nl}^* \left\{ \begin{array}{c} \delta q_{x_{\tau i}} \delta q_{x_{sj}} \\ \delta q_{y_{\tau i}} \delta q_{y_{sj}} \\ \delta q_{z_{\tau i}} \delta q_{z_{sj}} \end{array} \right\}
\tag{35}
$$

or rather

$$
\delta(\delta\boldsymbol{\epsilon}^T) = \left\{ \begin{array}{c} \delta q_{x_{\tau i}} \delta q_{x_{sj}} \\ \delta q_{y_{\tau i}} \delta q_{y_{sj}} \\ \delta q_{z_{\tau i}} \delta q_{z_{sj}} \end{array} \right\}^T (\mathbf{B}_{nl}^*)^T
\tag{36}
$$

where

$$
\mathbf{B}_{nl}^* = \left[\begin{array}{ccc}
F_{\tau_{,x}} F_{s_{,x}} N_i N_j & F_{\tau_{,x}} F_{s_{,x}} N_i N_j & F_{\tau_{,x}} F_{s_{,x}} N_i N_j \\
F_\tau F_s N_{i_{,y}} N_{j_{,y}} & F_\tau F_s N_{i_{,y}} N_{j_{,y}} & F_\tau F_s N_{i_{,y}} N_{j_{,y}} \\
F_{\tau_{,z}} F_{s_{,z}} N_i N_j & F_{\tau_{,z}} F_{s_{,z}} N_i N_j & F_{\tau_{,z}} F_{s_{,z}} N_i N_j \\
F_{\tau_{,x}} F_{s_{,z}} N_i N_j + F_{\tau_{,z}} F_{s_{,x}} N_i N_j & F_{\tau_{,x}} F_{s_{,z}} N_i N_j + F_{\tau_{,z}} F_{s_{,x}} N_i N_j & F_{\tau_{,x}} F_{s_{,z}} N_i N_j + F_{\tau_{,z}} F_{s_{,x}} N_i N_j \\
F_{\tau_{,z}} F_s N_i N_{j_{,y}} + F_\tau F_{s_{,z}} N_{i_{,y}} N_j & F_{\tau_{,z}} F_s N_i N_{j_{,y}} + F_\tau F_{s_{,z}} N_{i_{,y}} N_j & F_{\tau_{,z}} F_s N_i N_{j_{,y}} + F_\tau F_{s_{,z}} N_{i_{,y}} N_j \\
F_{\tau_{,x}} F_s N_i N_{j_{,y}} + F_\tau F_{s_{,x}} N_{i_{,y}} N_j & F_{\tau_{,x}} F_s N_i N_{j_{,y}} + F_\tau F_{s_{,x}} N_{i_{,y}} N_j & F_{\tau_{,x}} F_s N_i N_{j_{,y}} + F_\tau F_{s_{,x}} N_{i_{,y}} N_j
\end{array} \right]
\tag{37}
$$

Given Eq. (36) and after simple manipulations, the following passages are fairly clear:

$$
\begin{aligned}
< \delta(\delta\boldsymbol{\epsilon}^T)\boldsymbol{\sigma} > &= < \begin{Bmatrix} \delta q_{u_{x_{\tau i}}} \delta q_{u_{x_{sj}}} \\ \delta q_{u_{y_{\tau i}}} \delta q_{u_{y_{sj}}} \\ \delta q_{u_{z_{\tau i}}} \delta q_{u_{z_{sj}}} \end{Bmatrix}^T (\mathbf{B}^*_{nl})^T\boldsymbol{\sigma} > \\
&= \delta\mathbf{q}^T_{\tau i} < \text{diag}\left((\mathbf{B}^*_{nl})^T\boldsymbol{\sigma}\right) > \delta\mathbf{q}_{sj} \\
&= \delta\mathbf{q}^T_{\tau i} < \text{diag}\left((\mathbf{B}^*_{nl})^T(\boldsymbol{\sigma}_l + \boldsymbol{\sigma}_{nl})\right) > \delta\mathbf{q}_{sj} \\
&= \delta\mathbf{q}^T_{\tau i}(\mathbf{K}^{ij\tau s}_{\sigma_l} + \mathbf{K}^{ij\tau s}_{\sigma_{nl}})\delta\mathbf{q}_{sj} \\
&= \delta\mathbf{q}^T_{\tau i}\mathbf{K}^{ij\tau s}_{\sigma}\delta\mathbf{q}_{sj}
\end{aligned}
\tag{38}
$$

where $\text{diag}\left((\mathbf{B}^*_{nl})^T\boldsymbol{\sigma}\right)$ is the 3×3 diagonal matrix, whose diagonal terms are the components of the vector $(\mathbf{B}^*_{nl})^T\boldsymbol{\sigma}$. According to Eqs. (3) and (6), $\boldsymbol{\sigma}_l = \mathbf{C}\boldsymbol{\epsilon}_l$ and $\boldsymbol{\sigma}_{nl} = \mathbf{C}\boldsymbol{\epsilon}_{nl}$. The term elaborated in Eq. (38) defines a tangent term arising from the nonlinear form of the strain-displacement equations and is often called the geometric stiffness [63], of which $\mathbf{K}^{ij\tau s}_{\sigma} = \mathbf{K}^{ij\tau s}_{\sigma_l} + \mathbf{K}^{ij\tau s}_{\sigma_{nl}}$ is the fundamental nucleus. The explicit form of $\mathbf{K}^{ij\tau s}_{\sigma}$ is given in the following for the sake of completeness:

$$
\begin{aligned}
\mathbf{K}^{ij\tau s}_{\sigma} &= \big(< \sigma_{xx} F_{\tau,x} F_{s,x} N_i N_j > + < \sigma_{yy} F_\tau F_s N_{i,y} N_{j,x} > \\
&+ < \sigma_{zz} F_{\tau,z} F_{s,z} N_i N_j > + < \sigma_{xy} F_{\tau,x} F_s N_i N_{j,y} > \\
&+ < \sigma_{xy} F_\tau F_{s,x} N_{i,y} N_j > + < \sigma_{xz} F_{\tau,x} F_{s,z} N_i N_j > \\
&+ < \sigma_{xz} F_{\tau,z} F_{s,x} N_i N_j > + < \sigma_{yz} F_{\tau,z} F_s N_i N_{j,y} > \\
&+ < \sigma_{yz} F_\tau F_{s,z} N_{i,y} N_j > \big)\, \mathbf{I}
\end{aligned}
\tag{39}
$$

where $\mathbf{I}$ is the 3×3 identity matrix. Given $\mathbf{K}^{ij\tau s}_{T_1}$ and $\mathbf{K}^{ij\tau s}_{\sigma}$, the fundamental nucleus of the tangent stiffness matrix $\mathbf{K}^{ij\tau s}_{T}$ can be calculated straightforwardly (see Eq. (31)). It is now clear that this 3×3 matrix is the basic building block to be used for the formulation of the tangent stiffness matrix for any higher-order refined beam elements accounting for Green-Lagrange nonlinear strains. Readers can easily verify that the expansion of the FN of the tangent stiffness results into a symmetric element matrix. It is intended that, depending on the problem, the formulation of the fundamental nuclei of the secant and tangent stiffness matrices is much simplified if only some geometrical nonlinearities are retained, such as in the case of von Kármán nonlinearities.

6 Numerical results

In this section, various problems are addressed for demonstrating the capabilities of the present beam formulation to deal with classical as well as higher-order beam structural problems. First, large deflection and *elastica-like* analyses of one-dimensional solid cross-section structures are considered. Here, the attention is focussed on the capability of the proposed

	N. of beam elements	Beam theory order		
		Bilinear (1L4)	Quadratic (1L9)	Cubic (1L16)
$L/h = 10$	5	$0.540^{(8)}$	$0.582^{(12)}$	$0.582^{(12)}$
	10	$0.541^{(8)}$	$0.584^{(12)}$	$0.584^{(12)}$
	20	$0.541^{(8)}$	$0.584^{(12)}$	$0.585^{(13)}$
	40	$0.541^{(8)}$	$0.584^{(12)}$	$0.586^{(13)}$
$L/h = 100$	5	$0.549^{(8)}$	$0.596^{(12)}$	$0.596^{(12)}$
	10	$0.551^{(8)}$	$0.601^{(12)}$	$0.601^{(12)}$
	20	$0.552^{(8)}$	$0.603^{(12)}$	$0.603^{(12)}$
	40	$0.552^{(8)}$	$0.603^{(12)}$	$0.603^{(12)}$

Table 1: Normalized vertical displacement, u_z/L, of the square cross-section cantilever beam for $\frac{PL^2}{EI} = 3$. Reference solution from [5], $u_z/L = 0.603$. In brackets, the number of iterations to converge is given.

geometrically non-linear CUF beam model to account for slenderness effects, various boundary conditions and complex three-dimensional nonlinear stress states in a unified framework. The second part, by analyzing thin-walled beams, aims at assessing the refined capabilities of the LE kinematics, which can efficiently describe complex mechanical behaviors, such as coupled bending-torsion, localized buckling and warping. Whenever possible, the results are compared with those from the literature and commercial finite element tools.

6.1 Large deflection of cantilever beams

In the first analysis case, a cantilever, square cross-section beam subjected to large deflection due to a vertical loading is considered. The beam is made of an aluminum alloy with Young modulus E equal to 75 GPa and Poisson ratio $\nu = 0.33$. Various CUF-based LE beam models are considered in this analysis case. Namely, bilinear, quadratic, and cubic kinematics are employed, and they are obtained, respectively, by using one single L4, L9, and L16 Lagrange polynomial set to approximate the displacement field. The results reported hereby are compared to those from [5], where an analytical solution based on the Euler-Bernoulli Beam Model (EBBM) is devised.

Table 1 quotes the normalized vertical displacement, u_z/L, at the beam tip for various length-to-side ratio (L/h) and the loading condition $\frac{PL^2}{EI} = 3$, where P is the applied vertical load and $I = \frac{h^4}{12}$ is the second moment of area. In the table, the effect of the the mesh discretization (i.e., the number of B4 finite beam elements) on the solution is highlighted. Also, the number of iterations m to converge to solution $\mathbf{q}_m$ such that $\frac{|\mathbf{q}_m - \mathbf{q}_{m-1}|}{|\mathbf{q}_m|} < 0.01$ ($|\cdot|$ represents the l^2-norm) is given. In fact, a fixed-point (*Picard*) resolution algorithm that makes use only of $\mathbf{K}_S$ is employed for the results shown in Table 1.

Given the convergence of Table 1, 20 B4 finite elements along with a quadratic (1L9) beam theory are used for the subsequent analyses. Fig. 3 shows the equilibrium curves for short and slender beam structures, and the results of the present beam model are compared to those from linear and nonlinear (see [5]) EBBMs. From the solution iterates (circles in Fig. 3), it is clear that an arc-length method is used in this case to find the equilibrium curves of the 1L9 beam model. In the figure, also some relevant equilibrium deformation states are depicted.

The distribution along the thickness of the non-dimensional axial stress component, $\sigma_{yy}\frac{2I}{PLh}$,

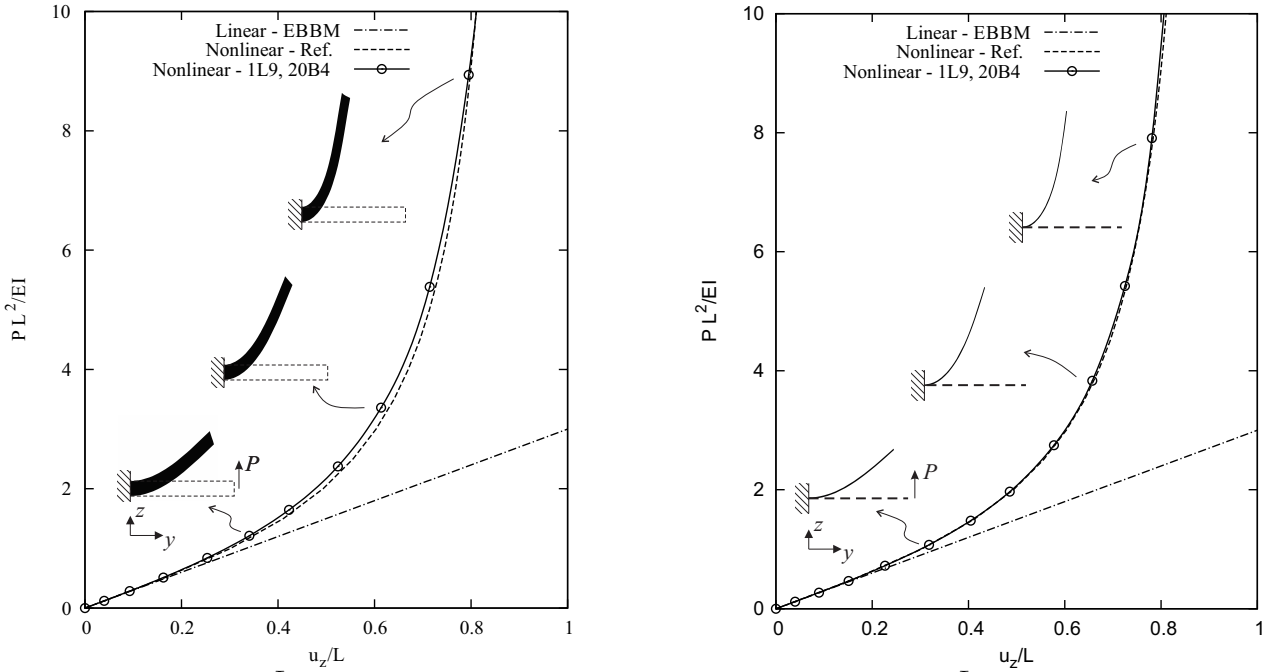

(a) $\frac{L}{h} = 10$ (b) $\frac{L}{h} = 100$

Figure 3: Equilibrium curves of the square cross-section beam subjected to vertical loading. Reference solution from [5].

on the clamped cross-section is also given in Fig. 4. In this figure, the solutions from both the nonlinear and linear analyses of the 1L9 beam model are given for various load levels and length-to-side ratios. In particular, the stress distributions are shown for the first load step and the same equilibrium states at which the deformed configurations are depicted in Fig. 3. It is clear that, as the loading is increased, the structure becomes dominated by traction. The following comments stem from this preliminary analysis:

- The proposed beam model can describe the large deflections of short and slender cantilever beams, in agreement with analytical reference results based on EBBM.
- The LE beam model is able to describe in an accurate manner the 3D stress/strain state.
- Classical beam theories may provide reliable results in terms of displacements. However, higher-order kinematics shall be used if accurate stress distribution of short beams is needed. In fact, as it is clear from Fig. 4(b), beam theories with first-order kinematics could reasonably approximate the axial stress distribution in the case of long beams. This aspect further justifies the assumptions of classical beam theories and their adoption to the analysis of thin structure. On the contrary, a first-order approximation may not be appropriate for the description of the stress state within short beams in bending (see Fig. 4(a)). Nevertheless, in both short and long beams, nonlinear geometrical effects cannot be neglected in the case of stress analysis of beams in large-rotations equilibrium states.

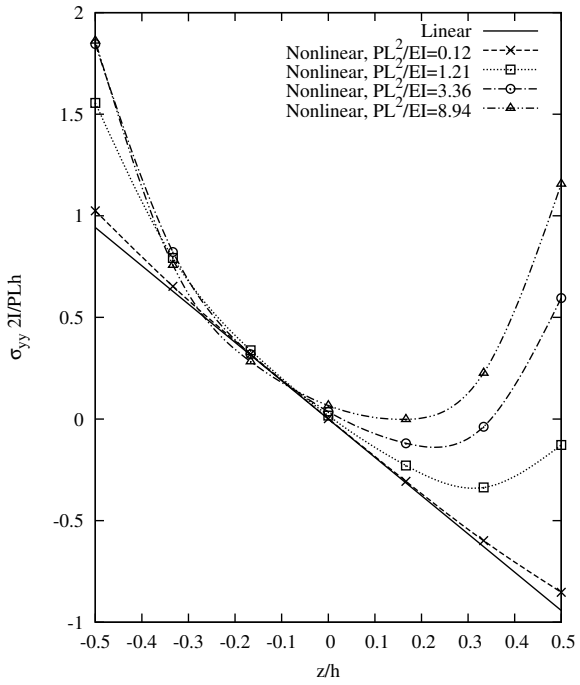

(a) $\frac{L}{h} = 10$

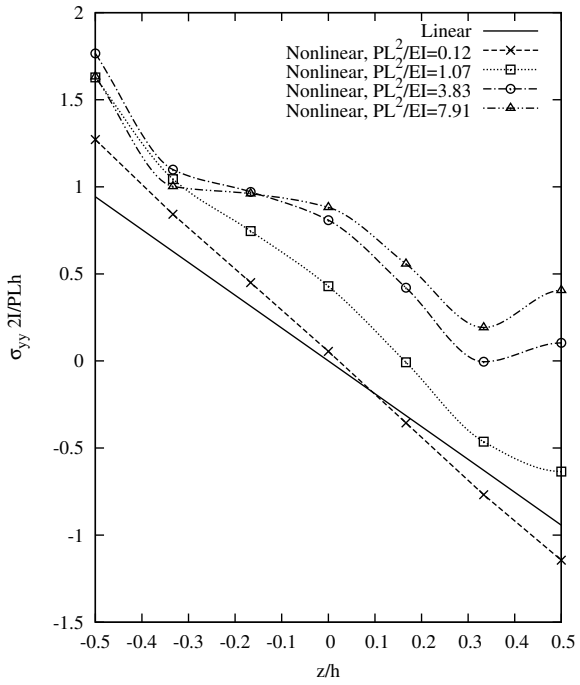

(b) $\frac{L}{h} = 100$

Figure 4: Through-the-thickness distribution of non-dimensional axial stress, $\sigma_{yy}\frac{2I}{PLh}$, on the clamped cross-section of the cantilever beam subjected to vertical loading; 1L9 model.

6.2 Post-buckling of beam-columns

The capability of the proposed geometrically-nonlinear unified formulation to deal with *elastica-like* problems is further demonstrated in this section. In fact, the post-buckling behavior of the same beam structure as considered in the previous analysis case is addressed.

First, the buckling loads of clamped-free and simply-supported beam-columns subjected to an axial load P are given in Tables 2 and 3 for the sake of completeness. In these tables, the results by various LE beam theories are normalized with the classical Euler critical load. Different slenderness ratios are considered, and 20B4 elements are used with reference to the present higher-order beam models, given the convergence analysis proposed in the previous section. The critical loads in Tables 2 and 3 have been calculated by linearizing the governing equations and evaluating the loads that make the linearized tangent stiffness matrix singular, i.e. $|\mathbf{K}_T| \approx |\mathbf{K}_0 + \mathbf{K}_{\sigma_l}| = 0$. As it is clear from the results, bilinear 1L4 beam theories overestimate the buckling loads. On the other hand, according to L9 and L16 higher-order kinematics, classical EBBM theory provides reliable results for moderately slender and slender structures.

Post-buckling equilibrium curves of the clamped-free and simply-supported configurations and $L/h = 100$ are respectively shown in Figs. 5 and 6, which give the axial and transverse displacements versus the loading P according to the higher-order 1L9 beam model. It must be clarified that in the case of the clamped-free beam, the displacements are measured at the free end. Contrarily, the displacements are measured at the mid-span in the case of the simply-supported beam. In both the configurations, the unstable solution branches have been *enforced* by applying a small load defect d as depicted in the figures and the arc-length method has been employed. In Figs. 5 and 6, some deformed configurations at notable equilibrium

	Beam theory order		
	Bilinear (1L4)	Quadratic (1L9)	Cubic (1L16)
L/h = 10	1.191	0.999	0.994
L/h = 100	1.197	1.003	1.003
L/h = 500	1.198	1.005	1.005

Table 2: Normalized critical buckling load, $\frac{4L^2}{\pi^2 EI}P_{cr}$, of the cantilever square cross-section beam subjected to compression.

	Beam theory order		
	Bilinear (1L4)	Quadratic (1L9)	Cubic (1L16)
L/h = 10	1.135	0.969	0.947
L/h = 100	1.194	1.000	1.000
L/h = 500	1.195	1.000	1.000

Table 3: Normalized critical buckling load, $\frac{L^2}{\pi^2 EI}P_{cr}$, of the simply-supported square cross-section beam subjected to compression.

statuses are also given and the results by the present beam formulation are compared to analytical EBBM solutions provided in [64]. It is rather clear that the proposed formulation can indistinctly deal with moderate and large deformations of buckled bars in a very accurate manner.

6.3 Thin-walled channel-section beams

In order to show the enhanced capabilities of the proposed refined nonlinear beam formulation, thin-walled symmetric and unsymmetric C-section cantilever beam structures are addressed as final examples. The beam whose cross-section geometry is shown in Fig. 7(a) is analysed first. The length of the beam is 0.9 m, whereas $h = 30$ cm, $w = 10$ cm, $t = 1.6$ cm, and $s = 1$ cm. The material adopted is such that $E = 21000$ kN/cm^2 and $\nu = 0.3$. Figure 7(a) also shows the position of the load P at the tip cross-section. The same problem was analysed by Gruttmann *et al.* in [27], whose results are used here for comparison purposes.

The vertical displacement component u_z at point A on the tip cross-section versus the load P is shown in Fig. 8, where the results from the present beam formulation are compared with those available from the literature. The LE beam model utilized for this analysis makes use of 6 L9 polynomials to approximate the kinematic field on the cross-section (see 7(b)), whereas 20 B4 finite elements are used along the beam axis. For the sake of completeness, some characteristic deformed configurations at important equilibrium states are depicted in Fig. 9. It must be underlined that the three-dimensional meshes illustrated in this figure are merely used for plotting convenience.

As a final example, the unsymmetric channel section beam whose cross-section is shown in Fig. 10 is further considered. The beam is made of the same aluminium alloy as used in the previous sections ($E = 75$ GPa, $\nu = 0.33$), it is 1 m long and is subjected to clamped-free boundary conditions. A loading P is applied at the free end as shown in Fig. 10. According to this figure, which also gives the cross-sectional dimensions, $w = 100$ mm, $h_1 = 48$ mm, $h_2 = 88$ mm, and $t = 8$ mm. Two different LE beam models are considered in this case.

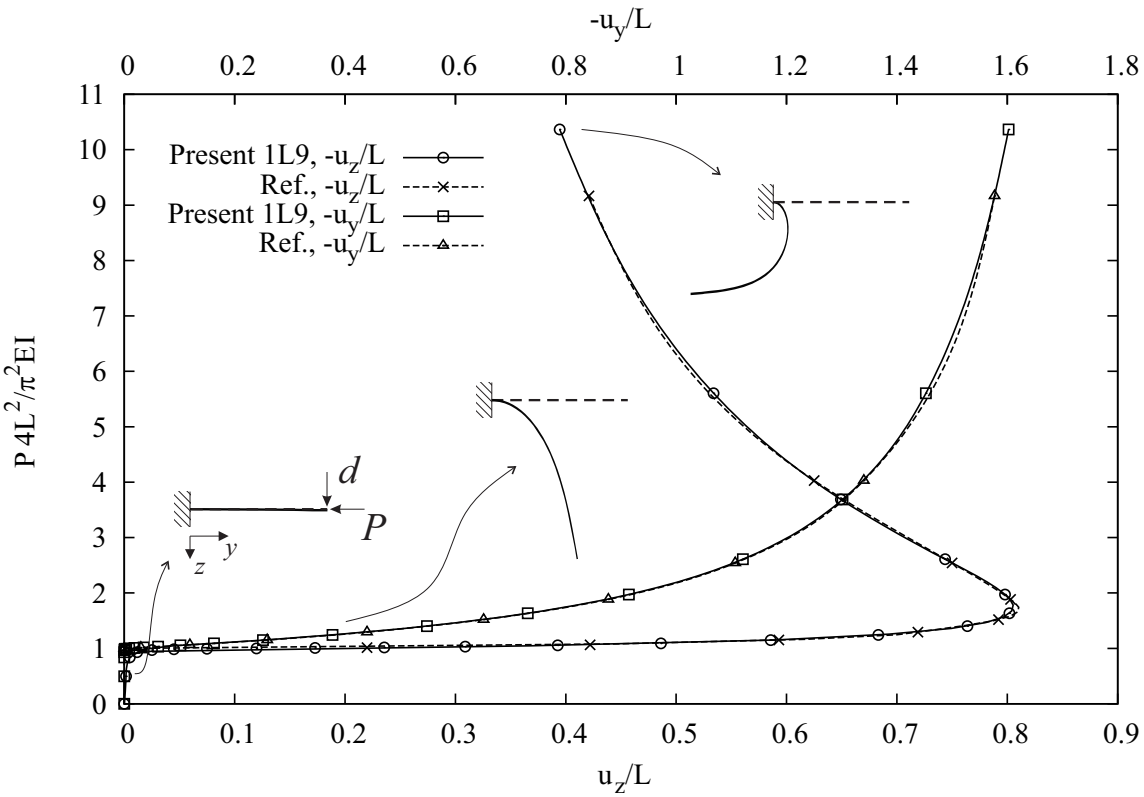

Figure 5: Post-buckling equilibrium curves of the cantilever square cross-section beam, $L/h = 100$ and $\frac{4L^2}{\pi^2 EI} d = 0.002$. Reference solution from [64].

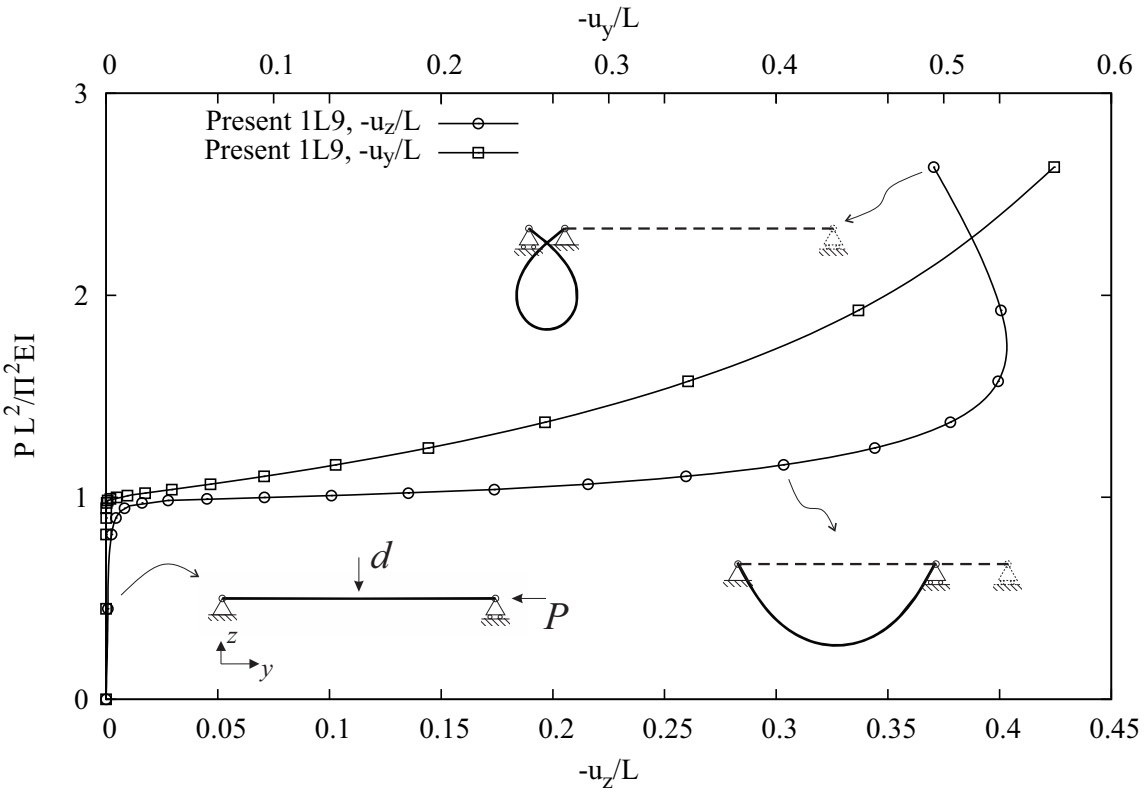

Figure 6: Post-buckling equilibrium curves of the simply-supported square cross-section beam, $L/h = 100$ and $\frac{L^2}{\pi^2 EI} d = 0.004$.

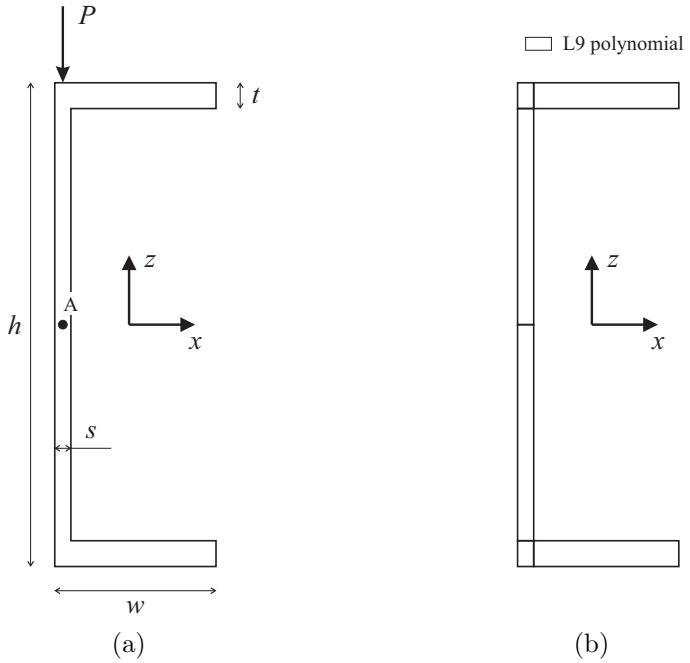

Figure 7: Cross-section geometry (a) and related 6L9 LE model subdomains discretization (b) of the symmetric channel-section beam.

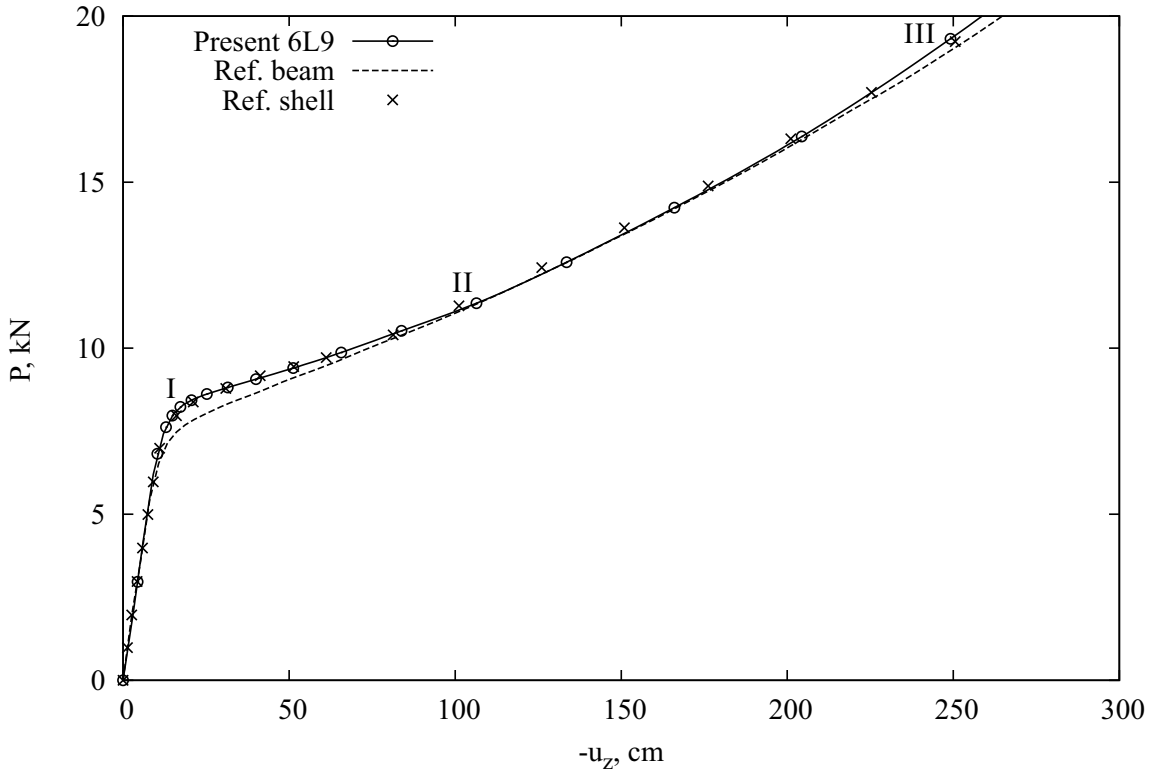

Figure 8: Equilibrium curves of the symmetric channel-section beam. Reference solutions from [27].

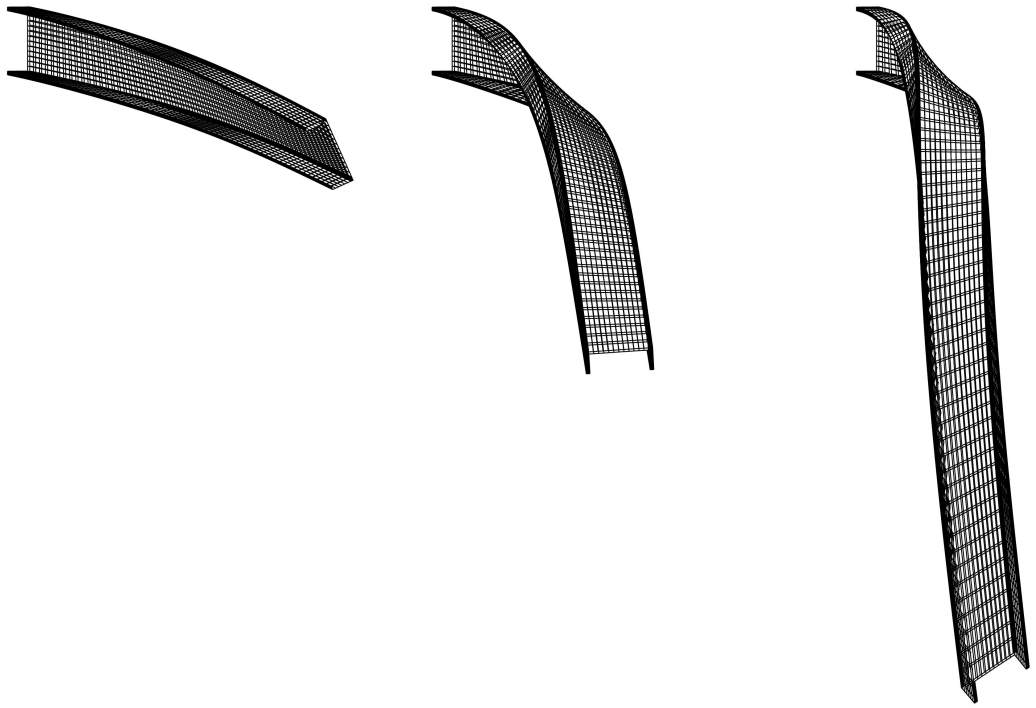

(a) $P = 8.23$ kN (b) $P = 11.35$ kN (c) $P = 19.32$ kN

Figure 9: Deformed configurations by 6L9 beam model of the symmetric channel section beam for equilibrium states I, II, and III.

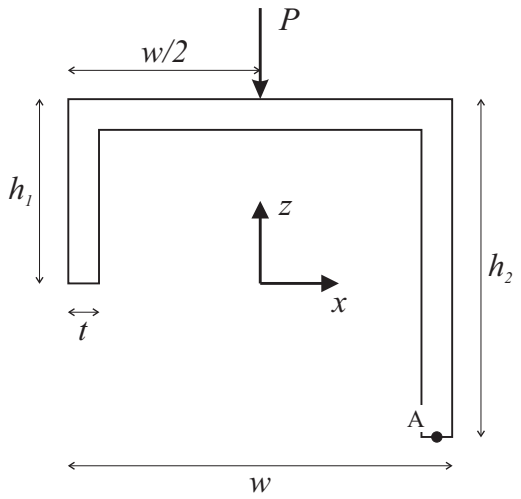

Figure 10: Cross-section geometry of the unsymmetric channel beam and loading condition.

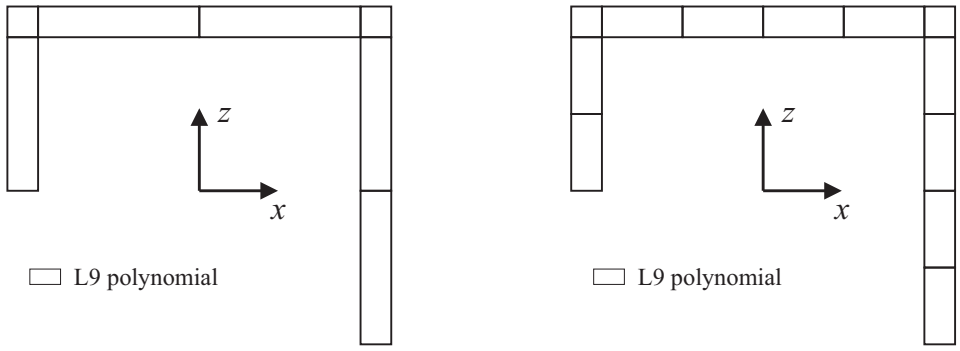

(a) 7L9 (b) 12L9

Figure 11: LE model subdomains discretization of the C-section beam.

Namely, a combination of 7 and 12 quadratic L9 polynomials are employed to discretize the beam kinematics on the beam cross-section. The two models are referred to as 7L9 and 12L9, respectively, and they are depicted in Fig. 11. On the other hand, 20 B4 beam elements are used along the axis for convergence reasons.

Figure 12(a) shows the equilibrium curves of the unsymmetric channel-section beam in the ranges of small and moderately large displacements. In this figure, the results of the present beam models are compared to a 3D elasticity solid model and a 2D plate model made with the commercial FE tool MSC.Nastran. In particular, given convergence analyses, the solid model was made of 10800 8-node CHEXA brick elements and 49995 Degrees of Freedom (DOFs). On the other hand, the 2D model was made of 5000 4-node CQUAD elements and 30906 DOFs. From Fig. 12(a), it is clear that both the MSC.Nastran models and the present 7L9 and 12L9 beam models, which present 8235 and 13725 DOFs respectively, give comparable results in the linear region. Contrarily, in the nonlinear range, the solutions from CUF-based LE models are very close to the solution given by the 3D solid model. In fact, unlike 2D plate FE models, both the LE beams and 3D solid elements make use of the full stress field in the calculation of the stiffness terms due to pre-stresses/geometrical nonlinearities. For the sake of completeness, Fig. 12(b) shows the equilibrium curves in the range of large displacements by the proposed higher-order beam models. In the same figure, the linear solutions are also given for comparison purposes. In Fig. 12(b), it is possible to identify three characteristic zones: (i) a linear and quasi/linear zone for $P \approx 0 \div 25$ kN; (ii) a softening zone in the interval $P \approx 25 \div 60$ kN; (iii) and an hardening zone for $P \gtrapprox 60$ kN. To better understand the kinematic evolution of the proposed problem in the large displacements domain, some selected deformed configurations of the C-section beam are depicted in Fig. 13 for equilibrium states I to VII (see Fig. 12(b)).

It is clear that the softening behavior that characterizes the channel-section beam problems discussed is due to two main effects. In the first problem (Fig. 7(a)), because of the asymmetry of the loading which is not applied in the shear center, the beam twists. As the beam twists, the bending stiffness decreases. In the second problem addressed in this section (Fig. 10), a major role is played by the local failure of the vertical flanges close to the clamped end at approximately $P = 30$ kN, see Fig. 13(b). It is obvious that, unlike bending-twisting coupling, this local phenomenon causing softening cannot be detected with classical beam

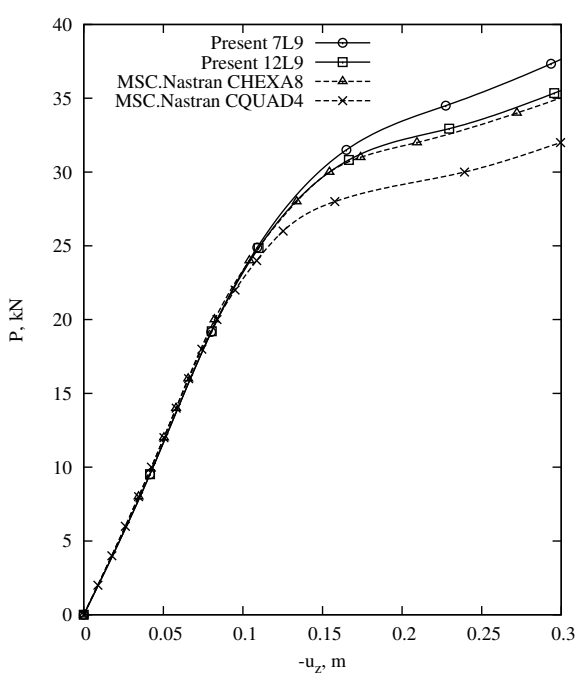

(a) Present beam vs MSC.Nastran models in the range of small and moderate displacements

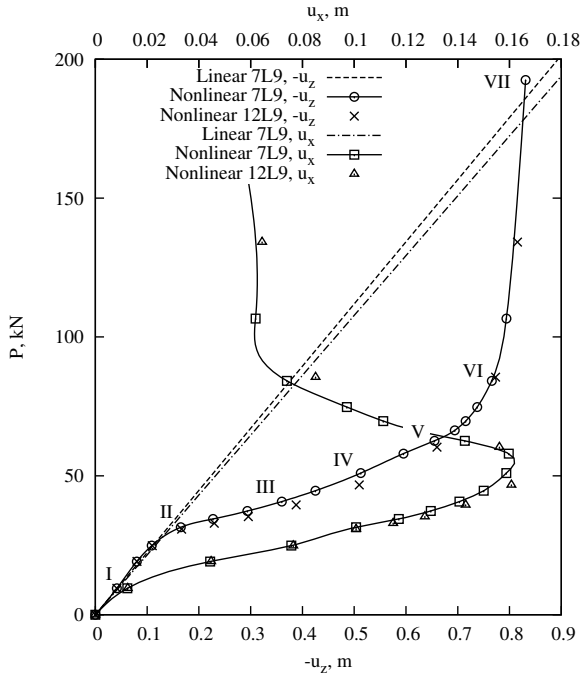

(b) Linear and nonlinear LE beam models in the range of large displacements

Figure 12: Displacement components at Point A on the tip cross-section versus load. Behavior of the unsymmetric C-section beam in the small/moderate (a) and large (b) displacements ranges.

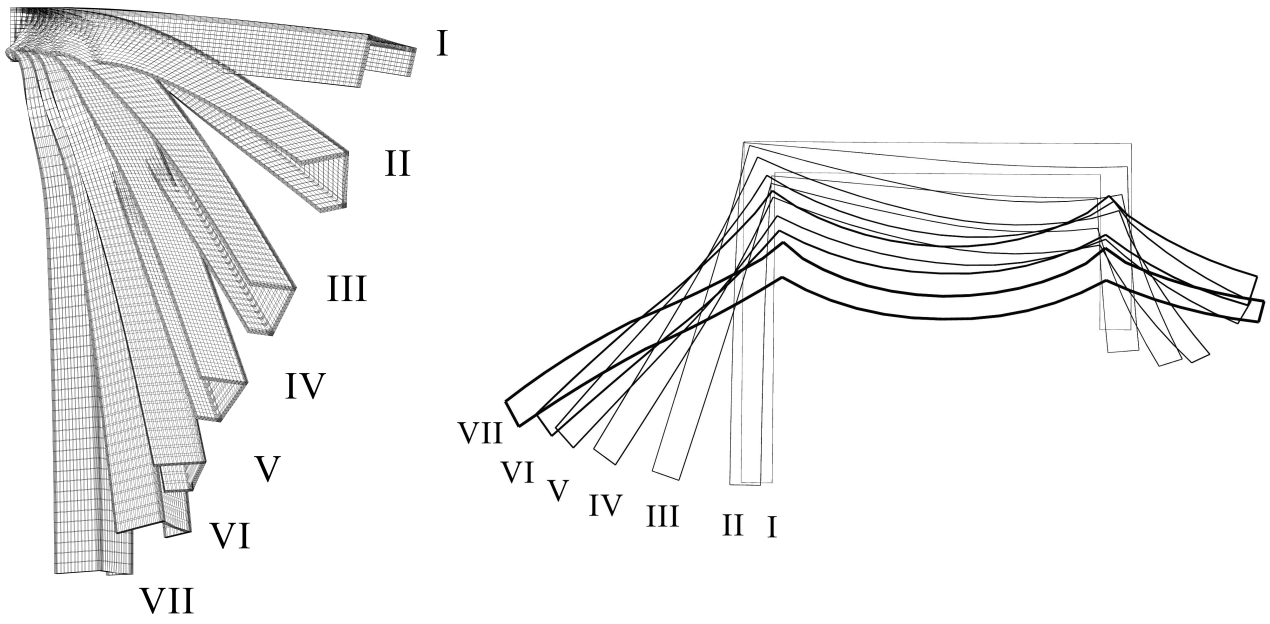

(a) (b)

Figure 13: Three-dimensional deformed configurations (a) and cross-sections at $y = 0.1$ m (b) for various load steps $P = [9.52, 31.50, 40.74, 51.00, 62.62, 84.21, 192.51]$ kN. Unsymmetric C-section beam, 7L9 model.

theories and more sophisticated models may be needed, such as 2D and 3D models or higher-order kinematics beam theories. For completeness reasons, it must be added that the sudden hardening which is shown in Fig. 12(b), is due to the fact that after the local failure of the beam at the clamped end and the consequent large displacements, the beam becomes subjected mainly to traction.

It is intended that the examples provided in this section have been discussed merely for assessing the present geometrically nonlinear formulation and for demonstrating that it can deal with very large displacements/rotations, bending-twisting couplings, localized phenomena and other higher-order effects accurately and with a number of DOFs which is much lower than those required by state-of-the-art FE models. Of course, the problems addressed here are also affected by very large strains (especially the second one) and more appropriate models should deal with plasticity also.

7 Conclusions

The unified formulation of geometrically nonlinear and elastic beam theory has been introduced in this work. By employing the Carrera Unified Formulation (CUF) and an extensive index notation, the kinematics of the generic beam model has been expressed as an arbitrary expansion of the primary mechanical unknowns. Then, the nonlinear governing equations and the related finite element approximation have been formulated using the principle of virtual work. The complete expressions of the secant (both in non-symmetric and symmetric forms) and tangent stiffness matrices of the unified beam element have been provided in terms of fundamental nuclei. A Newton-Raphson linearized incremental scheme along with an arc-length constraint relation have been used to solve the nonlinear algebraic system for several numerical cases. The results related to solid as well as thin-walled cross-section beam structures have widely demonstrated the versatility of the proposed methodology, which can indistinctly deal with large deformations/rotations and higher-order phenomena, such as nonlinear three-dimensional stress analysis, bending-torsion coupling, localized buckling, and warping, among the others. The research conducted provide enough confidence for future developments in this direction.

Appendix A Components of the secant stiffness matrix

According to Carrera *et al.* [44] and by using permutations, the fundamental nucleus of the stiffness matrix can be, in principle, defined by using only two independent components with no loss of generality. Nevertheless, for the sake of completeness and because in this paper the geometrically nonlinear stiffness terms in the domain of CUF are discussed for the first time, all the nine components for each of the nucleus sub-matrices are given.

The nine components of the 3×3 fundamental nucleus of the linear stiffness matrix are provided below in the form $\mathbf{K}_0^{ij\tau s}[r,c]$, where r is the row number ($r = 1,2,3$) and c is the column number ($c = 1,2,3$).

$$\begin{aligned}
\mathbf{K}_0^{ij\tau s}[1,1] &= < C_{11}\, F_{\tau,x}\, F_{s,x}\, N_i\, N_j > + < C_{44}\, F_{\tau,z}\, F_{s,z}\, N_i\, N_j > \\
&+ < C_{66}\, F_\tau\, F_s\, N_{i,y}\, N_{j,y} > \\
\mathbf{K}_0^{ij\tau s}[1,2] &= < C_{66}\, F_\tau\, F_{s,x}\, N_{i,y}\, N_j > + < C_{12}\, F_{\tau,x}\, F_s\, N_i\, N_{j,y} > \\
\mathbf{K}_0^{ij\tau s}[1,3] &= < C_{13}\, F_{\tau,x}\, F_{s,z}\, N_i\, N_j > + < C_{44}\, F_{\tau,z}\, F_{s,x}\, N_i\, N_j >
\end{aligned}$$

$$
\begin{aligned}
\mathbf{K}_0^{ij\tau s}[2,1] &= < C_{12}\, F_\tau\, F_{s,x}\, N_{i,y}\, N_j > + < C_{66}\, F_{\tau,x}\, F_s\, N_i\, N_{j,y} > \\
\mathbf{K}_0^{ij\tau s}[2,2] &= < C_{66}\, F_{\tau,x}\, F_{s,x}\, N_i\, N_j > + < C_{55}\, F_{\tau,z}\, F_{s,z}\, N_i\, N_j > \\
&+ < C_{22}\, F_\tau\, F_s\, N_{i,y}\, N_{j,y} > \\
\mathbf{K}_0^{ij\tau s}[2,3] &= < C_{23}\, F_\tau\, F_{s,z}\, N_{i,y}\, N_j > + < C_{55}\, F_{\tau,z}\, F_s\, N_i\, N_{j,y} > \\
\mathbf{K}_0^{ij\tau s}[3,1] &= < C_{44}\, F_{\tau,x}\, F_{s,z}\, N_i\, N_j > + < C_{13}\, F_{\tau,z}\, F_{s,x}\, N_i\, N_j > \\
\mathbf{K}_0^{ij\tau s}[3,2] &= < C_{55}\, F_\tau\, F_{s,z}\, N_{i,y}\, N_j > + < C_{23}\, F_{\tau,z}\, F_s\, N_i\, N_{j,y} > \\
\mathbf{K}_0^{ij\tau s}[3,3] &= < C_{44}\, F_{\tau,x}\, F_{s,x}\, N_i\, N_j > + < C_{33}\, F_{\tau,z}\, F_{s,z}\, N_i\, N_j > \\
&+ < C_{55}\, F_\tau\, F_s\, N_{i,y}\, N_{j,y} >
\end{aligned}
$$

Similarly, the components of the fundamental nucleus of the first-order nonlinear stiffness matrix $\mathbf{K}_{nll}^{ij\tau s}$ are:

For $c = 1$:

$$
\begin{aligned}
\mathbf{K}_{nll}^{ij\tau s}[r,c] &= < \mathbf{u}_{,x}[r]\, C_{11}\, F_{\tau,x}\, F_{s,x}\, N_i\, N_j > + < \mathbf{u}_{,x}[r]\, C_{44}\, F_{\tau,z}\, F_{s,z}\, N_i\, N_j > \\
&+ < \mathbf{u}_{,x}[r]\, C_{66}\, F_\tau\, F_s\, N_{i,y}\, N_{j,y} > + < \mathbf{u}_{,y}[r]\, C_{66}\, F_{\tau,x}\, F_s\, N_i\, N_{j,y} > \\
&+ < \mathbf{u}_{,x}[r]\, C_{12}\, F_\tau\, F_{s,x}\, N_{i,y}\, N_j > + < \mathbf{u}_{,z}[r]\, C_{44}\, F_{\tau,x}\, F_{s,z}\, N_i\, N_j > \\
&+ < \mathbf{u}_{,z}[r]\, C_{13}\, F_{\tau,z}\, F_{s,x}\, N_i\, N_j >
\end{aligned}
$$

For $c = 2$:

$$
\begin{aligned}
\mathbf{K}_{nll}^{ij\tau s}[r,c] &= < \mathbf{u}_{,x}[r]\, C_{12}\, F_{\tau,x}\, F_s\, N_i\, N_{j,y} > + < \mathbf{u}_{,x}[r]\, C_{66}\, F_\tau\, F_{s,x}\, N_{i,y}\, N_j > \\
&+ < \mathbf{u}_{,y}[r]\, C_{66}\, F_{\tau,x}\, F_{s,x}\, N_i\, N_j > + < \mathbf{u}_{,y}[r]\, C_{55}\, F_{\tau,z}\, F_{s,z}\, N_i\, N_j > \\
&+ < \mathbf{u}_{,y}[r]\, C_{22}\, F_\tau\, F_s\, N_{i,y}\, N_{j,y} > + < \mathbf{u}_{,z}[r]\, C_{23}\, F_{\tau,z}\, F_s\, N_i\, N_{j,y} > \\
&+ < \mathbf{u}_{,z}[r]\, C_{55}\, F_\tau\, F_{s,z}\, N_{i,y}\, N_j >
\end{aligned}
$$

For $c = 3$:

$$
\begin{aligned}
\mathbf{K}_{nll}^{ij\tau s}[r,c] &= < \mathbf{u}_{,x}[r]\, C_{13}\, F_{\tau,x}\, F_{s,z}\, N_i\, N_j > + < \mathbf{u}_{,x}[r]\, C_{44}\, F_{\tau,z}\, F_{s,x}\, N_i\, N_j > \\
&+ < \mathbf{u}_{,y}[r]\, C_{55}\, F_{\tau,z}\, F_s\, N_i\, N_{j,y} > + < \mathbf{u}_{,y}[r]\, C_{23}\, F_\tau\, F_{s,z}\, N_{i,y}\, N_j > \\
&+ < \mathbf{u}_{,z}[r]\, C_{44}\, F_{\tau,x}\, F_{s,x}\, N_i\, N_j > + < \mathbf{u}_{,z}[r]\, C_{33}\, F_{\tau,z}\, F_{s,z}\, N_i\, N_j > \\
&+ < \mathbf{u}_{,z}[r]\, C_{55}\, F_\tau\, F_s\, N_{i,y}\, N_{j,y} >
\end{aligned}
$$

The components of $\mathbf{K}_{lnl}^{ij\tau s}$ are not given here, but they can be easily obtained from $\mathbf{K}_{nll}^{ij\tau s}$. In fact, it is clear from Eq. (30) that $\left(\mathbf{K}_{lnl}^{ij\tau s}\right)^T = \frac{1}{2}\mathbf{K}_{nll}^{ij\tau s}$.

Finally, the generic component $[r,c]$ of the matrix $\mathbf{K}_{nlnl}^{ij\tau s}$ is summarized in the following:

$$
\begin{aligned}
2 \times \mathbf{K}_{nlnl}^{ij\tau s}[r,c] &= < \mathbf{u}_{,x}[r]\, \mathbf{u}_{,x}[c]\, C_{11}\, F_{\tau,x}\, F_{s,x}\, N_i\, N_j > + < \mathbf{u}_{,x}[r]\, \mathbf{u}_{,x}[c]\, C_{44}\, F_{\tau,z}\, F_{s,z}\, N_i\, N_j > \\
&+ < \mathbf{u}_{,x}[r]\, \mathbf{u}_{,x}[c]\, C_{66}\, F_\tau\, F_s\, N_{i,y}\, N_{j,y} > + < \mathbf{u}_{,y}[r]\, \mathbf{u}_{,y}[c]\, C_{66}\, F_{\tau,x}\, F_{s,x}\, N_i\, N_j > \\
&+ < \mathbf{u}_{,y}[r]\, \mathbf{u}_{,y}[c]\, C_{55}\, F_{\tau,z}\, F_{s,z}\, N_i\, N_j > + < \mathbf{u}_{,y}[r]\, \mathbf{u}_{,y}[c]\, C_{22}\, F_\tau\, F_s\, N_{i,y}\, N_{j,y} > \\
&+ < \mathbf{u}_{,z}[r]\, \mathbf{u}_{,z}[c]\, C_{44}\, F_{\tau,x}\, F_{s,x}\, N_i\, N_j > + < \mathbf{u}_{,z}[r]\, \mathbf{u}_{,z}[c]\, C_{33}\, F_{\tau,z}\, F_{s,z}\, N_i\, N_j > \\
&+ < \mathbf{u}_{,z}[r]\, \mathbf{u}_{,z}[c]\, C_{55}\, F_\tau\, F_s\, N_{i,y}\, N_{j,y} > + < \mathbf{u}_{,x}[r]\, \mathbf{u}_{,y}[c]\, C_{12}\, F_{\tau,x}\, F_s\, N_i\, N_{j,y} > \\
&+ < \mathbf{u}_{,x}[r]\, \mathbf{u}_{,y}[c]\, C_{66}\, F_\tau\, F_{s,x}\, N_{i,y}\, N_j > + < \mathbf{u}_{,y}[r]\, \mathbf{u}_{,x}[c]\, C_{12}\, F_\tau\, F_{s,x}\, N_{i,y}\, N_j > \\
&+ < \mathbf{u}_{,y}[r]\, \mathbf{u}_{,x}[c]\, C_{66}\, F_{\tau,x}\, F_s\, N_i\, N_{j,y} > + < \mathbf{u}_{,x}[r]\, \mathbf{u}_{,z}[c]\, C_{13}\, F_{\tau,x}\, F_{s,z}\, N_i\, N_j > \\
&+ < \mathbf{u}_{,x}[r]\, \mathbf{u}_{,z}[c]\, C_{44}\, F_{\tau,z}\, F_{s,x}\, N_i\, N_j > + < \mathbf{u}_{,z}[r]\, \mathbf{u}_{,x}[c]\, C_{13}\, F_{\tau,z}\, F_{s,x}\, N_i\, N_j > \\
&+ < \mathbf{u}_{,z}[r]\, \mathbf{u}_{,x}[c]\, C_{44}\, F_{\tau,x}\, F_{s,z}\, N_i\, N_j > + < \mathbf{u}_{,y}[r]\, \mathbf{u}_{,z}[c]\, C_{23}\, F_\tau\, F_{s,z}\, N_{i,y}\, N_j > \\
&+ < \mathbf{u}_{,y}[r]\, \mathbf{u}_{,z}[c]\, C_{55}\, F_{\tau,z}\, F_s\, N_i\, N_{j,y} > + < \mathbf{u}_{,z}[r]\, \mathbf{u}_{,y}[c]\, C_{55}\, F_\tau\, F_{s,z}\, N_{i,y}\, N_j > \\
&+ < \mathbf{u}_{,z}[r]\, \mathbf{u}_{,y}[c]\, C_{23}\, F_{\tau,z}\, F_s\, N_i\, N_{j,y} >
\end{aligned}
$$

In the expressions above, $\mathbf{u}_{,x}[r]$ represents the r-th component of the vector $\dfrac{\partial \mathbf{u}}{\partial x}$; e.g. $\mathbf{u}_{,x}[2] = u_{y,x}$. Analogously, $\mathbf{u}_{,y}[c]$ is the c-th component of the vector $\dfrac{\partial \mathbf{u}}{\partial y}$, etc.

Appendix B On the non-symmetry of the secant stiffness matrix

Equations (29) and (30) reveal that the secant stiffness matrix $\mathbf{K}_S$ is not symmetric because $\left(\mathbf{K}_{lnl}^{ij\tau s}\right)^T = \frac{1}{2}\mathbf{K}_{nll}^{ij\tau s}$. According to [65] and within the domain of finite element applications, the non-symmetry of the secant stiffness matrix comports two main drawbacks. First, ad-hoc assembly techniques must be devised, and the whole matrix needs to be stored. This would seriously affect in a negative manner both the calculation times and the memory usage. Second, in the case in which the secant stiffness matrix is used instead of the tangent stiffness matrix in the linearized incremental problem of Eq. (18), for example in *secant methods*, dedicated algorithms for the resolutions of the linear systems must be adopted. Indeed, algorithms available in finite element tools are commonly made for symmetric matrices.

To overcome the aforementioned problems, in the past and recent literature, some authors have explored new possibilities of formulating symmetric forms of the secant stiffness matrix for a larger variety of problems, see for example [66, 67, 68, 62, 69]. In fact, according to the pioneering work of Rajasekaran and Murray [70] who, in investigating the incremental approach that Mallet and Marcal [71] introduced for the resolution of a *total Lagrangian* FEM-based formulation of a nonlinear structural problem, noticed that the expression of $\mathbf{K}_S$ is not uniquely determined.

In the present work, according to [65, 72], a symmetric form of the secant stiffness matrix is devised by expressing the virtual variation of the internal strain energy due by the contribution $\mathbf{K}_{nll}^{ij\tau s}$ as follows:

$$\begin{aligned}(\delta L_{\text{int}})_{nll} &= < \delta\, \boldsymbol{\epsilon}_{nl}^T\, \boldsymbol{\sigma}_l > \\ &= \frac{1}{2} < \delta \boldsymbol{\epsilon}_{nl}^T\, \mathbf{C}\, \boldsymbol{\epsilon}_l + \delta \boldsymbol{\epsilon}_{nl}^T\, \boldsymbol{\sigma}_l > \\ &= \frac{1}{2}\delta \mathbf{q}_{\tau i}^T (\mathbf{K}_{nll}^{ij\tau s} + \mathbf{K}_{\sigma_l}^{ij\tau s})\mathbf{q}_{si}\end{aligned}$$

Thus, following Eq. (29), the total virtual variation of the strain energy is

$$\delta L_{\text{int}} = \delta \mathbf{q}_{\tau i}^T (\mathbf{K}_0^{ij\tau s} + \mathbf{K}_{lnl}^{ij\tau s} + \frac{1}{2}\mathbf{K}_{nll}^{ij\tau s} + \frac{1}{2}\mathbf{K}_{\sigma_l}^{ij\tau s} + \mathbf{K}_{nlnl}^{ij\tau s})\mathbf{q}_{si}$$

Or, in other words,

$$\mathbf{K}_S^{ij\tau s} = \mathbf{K}_0^{ij\tau s} + \mathbf{K}_{lnl}^{ij\tau s} + \frac{1}{2}\mathbf{K}_{nll}^{ij\tau s} + \frac{1}{2}\mathbf{K}_{\sigma_l}^{ij\tau s} + \mathbf{K}_{nlnl}^{ij\tau s} = \mathbf{K}_0^{ij\tau s} + \frac{1}{2}(\mathbf{K}_{T1}^{ij\tau s} + \mathbf{K}_{\sigma_l}^{ij\tau s})$$

The expansion of the fundamental nucleus of the secant stiffness matrix as given above results now into a symmetric matrix.

References

[1] A. E. H. Love. *A treatise on the mathematical theory of elasticity.* Cambridge University Press, Cambridge, UK, 2013.

[2] R. Frisch-Fay. *Flexible bars*. Butterworths, Washington D.C., USA, 1962.

[3] S.P. Timoshenko and J.M. Gere. *Theory of elastic stability*. Tokyo, 1961.

[4] L. Euler. *De curvis elasticis*. Lausanne and Geneva: Bousquet, 1744.

[5] K. E. Bisshopp and D. C. Drucker. Large deflection of cantilever beams. *Quarterly of Applied Mathematics*, 3(3):272–275, 1945.

[6] C. Y. Wang. Post-buckling of a clamped-simply supported elastica. *International Journal of Non-Linear Mechanics*, 32(6):1115–1122, 1997.

[7] H. H. Denman and R. Schmidt. Chebyshev approximation applied to large deflections of elastica. *Industrial Mathematics*, 18:63–74, 1968.

[8] T. M. Wang, S. L. Lee, and O. C. Zienkiewicz. A numerical analysis of large deflections of beams. *International Journal of Mechanical Sciences*, 3(3):219–228, 1961.

[9] Z. P. Bažant and L. Cedolin. *Stability of structures: elastic, inelastic, fracture and damage theories*. World Scientific, Singapore, 2010.

[10] J. H. Argyris, P. C. Dunne, G. Malejannakis, and D. W. Scharpf. On large displacement-small strain analysis of structures with rotational degrees of freedom. *Computer Methods in Applied Mechanics and Engineering*, 15(1):99–135, 1978.

[11] J. H. Argyris, O. Hilpert, G. A. Malejannakis, and D. W. Scharpf. On the geometrical stiffness of a beam in space - a consistent v.w. approach. *Computer Methods in Applied Mechanics and Engineering*, 20(1):105–131, 1979.

[12] K.-J. Bathe and S. Bolourchi. Large displacement analysis of three-dimensional beam structures. *International Journal for Numerical Methods in Engineering*, 14(7):961–986, 1979.

[13] M. A. Crisfield. A consistent co-rotational formulation for non-linear, three-dimensional, beam-elements. *Computer Methods in Applied Mechanics and Engineering*, 81(2):131–150, 1990.

[14] E. Reissner. On finite deformations of space-curved beams. *Zeitschrift für angewandte Mathematik und Physik ZAMP*, 32(6):734–744, 1981.

[15] J. C. Simo and L. Vu-Quoc. A three-dimensional finite-strain rod model. Part ii: Computational aspects. *Computer Methods in Applied Mechanics and Engineering*, 58(1):79–116, 1986.

[16] J. C. Simo and L. Vu-Quoc. A geometrically-exact rod model incorporating shear and torsion-warping deformation. *International Journal of Solids and Structures*, 27(3):371–393, 1991.

[17] A. Cardona and M. Géradin. A beam finite element non-linear theory with finite rotations. *International journal for Numerical Methods in Engineering*, 26(11):2403–2438, 1988.

[18] A. Ibrahimbegović, F. Frey, and I. Kožar. Computational aspects of vector-like parametrization of three-dimensional finite rotations. *International Journal for Numerical Methods in Engineering*, 38(21):3653–3673, 1995.

[19] Y.-B. Yang, J.-D. Yau, and L.-J. Leu. Recent developments in geometrically nonlinear and postbuckling analysis of framed structures. *Applied Mechanics Reviews*, 56(4):431–449, 2003.

[20] J.-X. Gu and S.-L. Chan. A refined finite element formulation for flexural and torsional buckling of beam–columns with finite rotations. *Engineering Structures*, 27(5):749–759, 2005.

[21] S. P. Timoshenko. On the transverse vibrations of bars of uniform cross section. *Philosophical Magazine*, 43:125–131, 1922.

[22] E. Reissner. On one-dimensional large-displacement finite-strain beam theory. *Studies in Applied Mathematics*, 52(2):87–95, 1973.

[23] E. Reissner. Some considerations on the problem of torsion and flexure of prismatical beams. *International Journal of Solids and Structures*, 15(1):41–53, 1979.

[24] E. Reissner. Further considerations on the problem of torsion and flexure of prismatical beams. *International Journal of Solids and Structures*, 19(5):385–392, 1983.

[25] P. F. Pai and A. N. Palazotto. Large-deformation analysis of flexible beams. *International Journal of Solids and Structures*, 33(9):1335–1353, 1996.

[26] A. Mohyeddin and A. Fereidoon. An analytical solution for the large deflection problem of timoshenko beams under three-point bending. *International Journal of Mechanical Sciences*, 78:135–139, 2014.

[27] F. Gruttmann, R. Sauer, and W. Wagner. A geometrical nonlinear eccentric 3d-beam element with arbitrary cross-sections. *Computer Methods in Applied Mechanics and Engineering*, 160(3):383–400, 1998.

[28] W. Yu, V. V. Volovoi, D. H. Hodges, and X. Hong. Validation of the variational asymptotic beam sectional analysis (VABS). *AIAA Journal*, 40:2105–2113, 2002.

[29] W. Yu, D. H. Hodges, V. V. Volovoi, and E. D. Fuchs. A generalized vlasov theory for composite beams. *Thin-Walled Structures*, 43(9):1493–1511, 2005.

[30] E. Carrera, A. Pagani, M. Petrolo, and E. Zappino. Recent developments on refined theories for beams with applications. *Mechanical Engineering Reviews*, 2(2):1–30, 2015.

[31] V. Z. Vlasov. *Thin-walled elastic beams*. National Science Foundation, Washington, 1961.

[32] F. Bleich. *Buckling strength of metal structures*. McGraw-Hill, 1952.

[33] N. W. Murray. *Introduction to the Theory of Thin-Walled Structures*. Oxford University Press, New York, 1984.

[34] A. Genoese, A. Genoese, A. Bilotta, and G. Garcea. A geometrically exact beam model with non-uniform warping coherently derived from the saint venant rod. *Engineering Structures*, 68:33–46, 2014.

[35] C. Basaglia, D. Camotim, and N. Silvestre. Post-buckling analysis of thin-walled steel frames using generalised beam theory (gbt). *Thin-Walled Structures*, 62:229–242, 2013.

[36] S. P. Machado. Non-linear buckling and postbuckling behavior of thin-walled beams considering shear deformation. *International Journal of Non-Linear Mechanics*, 43(5):345–365, 2008.

[37] F. Mohri, A. Eddinari, N. Damil, and M. P. Ferry. A beam finite element for non-linear analyses of thin-walled elements. *Thin-Walled Structures*, 46(7):981–990, 2008.

[38] F. Mohri, S. A. Meftah, and N. Damil. A large torsion beam finite element model for tapered thin-walled open cross sections beams. *Engineering Structures*, 99:132–148, 2015.

[39] E. J. Sapountzakis and V. J. Tsipiras. Non-linear elastic non-uniform torsion of bars of arbitrary cross-section by bem. *International Journal of Non-Linear Mechanics*, 45(1):63–74, 2010.

[40] E. J. Sapountzakis and J. A. Dourakopoulos. Flexural-torsional postbuckling analysis of beams of arbitrary cross section. *Acta mechanica*, 209(1-2):67–84, 2010.

[41] R. F. Vieira, F. B. E. Virtuoso, and E. B. R. Pereira. A higher order beam model for thin-walled structures with in-plane rigid cross-sections. *Engineering Structures*, 84:1–18, 2015.

[42] G. Garcea, L. Leonetti, and D. Magisano. Advantages of the mixed format in geometrically nonlinear analysis of beams and shells using solid finite elements. *International Journal for Numerical Methods in Engineering*, 2016.

[43] E. Carrera, G. Giunta, and M. Petrolo. *Beam Structures: Classical and Advanced Theories*. John Wiley & Sons, 2011.

[44] E. Carrera, M. Cinefra, M. Petrolo, and E. Zappino. *Finite Element Analysis of Structures through Unified Formulation*. John Wiley & Sons, Chichester, West Sussex, UK., 2014.

[45] E. Carrera, A. Pagani, and M. Petrolo. Classical, refined and component-wise theories for static analysis of reinforced-shell wing structures. *AIAA Journal*, 51(5):1255–1268, 2013.

[46] E. Carrera and A. Pagani. Accurate response of wing structures to free vibration, load factors and non-structural masses. *AIAA Journal*, 54(1):227–241, 2016.

[47] E. Carrera, A. Pagani, and M. Petrolo. Refined 1D finite elements for the analysis of secondary, primary, and complete civil engineering structures. *Journal of Structural Engineering*, 141:04014123/1–14, 2015.

[48] E. Carrera and A. Pagani. Free vibration analysis of civil engineering structures by component-wise models. *Journal of Sound and Vibration*, 333(19):4597–4620, 2014.

[49] E. Carrera, M. Filippi, P. K. R. Mahato, and A. Pagani. Advanced models for free vibration analysis of laminated beams with compact and thin-walled open/closed sections. *Journal of Composite Materials*, 49(17):2085–2101, 2014.

[50] E. Carrera and M. Petrolo. Guidelines and recommendations to construct theories for metallic and composite plates. *AIAA Journal*, 48(12):2852–2866, 2010. doi: 10.2514/1.J050316.

[51] K. J. Bathe. *Finite element procedure*. Prentice hall, Upper Saddle River, New Jersey, USA, 1996.

[52] E. Carrera and M. Petrolo. Refined beam elements with only displacement variables and plate/shell capabilities. *Meccanica*, 47(3):537–556, 2012.

[53] K. Washizu. *Variational Methods in Elasticity and Plasticity*. Pergamon, Oxford, 1968.

[54] J. N. Reddy. *An Introduction to Nonlinear Finite Element Analysis: with applications to heat transfer, fluid mechanics, and solid mechanics*. Oxford University Press, Oxford, 2014.

[55] E. Carrera. A study on arc-length-type methods and their operation failures illustrated by a simple model. *Computers & Structures*, 50(2):217–229, 1994.

[56] M. A. Crisfield. *Non-linear Finite Element Analysis of Solid and Structures*. John Wiley & Sons, Chichester, England, 1991.

[57] M. A. Crisfield. A fast incremental/iterative solution procedure that handles "snap-through". *Computers & Structures*, 13(1):55–62, 1981.

[58] M. A. Crisfield. An arc-length method including line searches and accelerations. *International journal for numerical methods in engineering*, 19(9):1269–1289, 1983.

[59] J.-L Batoz and G. Dhatt. Incremental displacement algorithms for nonlinear problems. *International Journal for Numerical Methods in Engineering*, 14(8):1262–1267, 1979.

[60] K. H. Schweizerhof and P. Wriggers. Consistent linearization for path following methods in nonlinear fe analysis. *Computer Methods in Applied Mechanics and Engineering*, 59(3):261–279, 1986.

[61] P. Wriggers and J. C. Simo. A general procedure for the direct computation of turning and bifurcation points. *International Journal for Numerical Methods in Engineering*, 30(1):155–176, 1990.

[62] E. Oñate. On the derivation and possibilities of the secant stiffness matrix for non linear finite element analysis. *Computational Mechanics*, 15(6):572–593, 1995.

[63] O. C. Zienkiewicz and R. L. Taylor. *The Finite Element Method for Solid and Structural Mechanics*. Butterworth-Heinemann, Washington, 6th edition, 2005.

[64] S. P. Timoshenko and J. N. Goodier. *Theory of elasticity*. McGraw-Hill, 1970.

[65] E. Carrera. Sull'uso dell'operatore secante in analisi non lineare di strutture multistrato con il metodo degli elementi finiti. In *XI Congresso Nazionale AIMETA, Trento*, 28 September - 2 October 1992.

[66] R. D. Wood and B. Schrefler. Geometrically non-linear analysis–a correlation of finite element notations. *International Journal for Numerical Methods in Engineering*, 12(4):635–642, 1978.

[67] C. Felippa and L. A. Crivelli. The core-congruential formulation of geometrically nonlinear finite elements. In P. Wriggers and W. Wagner, editors, *Non Linear Computational Mechanics. The State of the Art*. Springer, Berlin, 1991.

[68] M. Badawi and A. R. Cusens. Symmetry of the stiffness matrices for geometrically non-linear analysis. *Communications in Applied Numerical Methods*, 8(2):135–140, 1992.

[69] A. Morán, E. Oñate, and J. Miquel. A general procedure for deriving symmetric expressions for the secant and tangent stiffness matrices in finite element analysis. *International Journal for Numerical Methods in Engineering*, 42(2):219–236, 1998.

[70] S. Rajasekaran and D. W. Murray. Incremental finite element matrices. *Journal of the Structural Division*, 99(12):2423–2438, 1973.

[71] R. H. Mallett and P. V. Marcal. Finite element analysis of nonlinear structures. *Journal of the Structural Division*, 94(9):2081–2105, 1968.

[72] E. Carrera. *Comportamento Postcritico di Gusci Multistrato*. PhD thesis, Department of Aerospace Engineering, Politecnico di Torino, 1991.